J. Fluid Mech. (2014), *vol.* 752, *pp.* 184–218. © Cambridge University Press 2014
doi:10.1017/jfm.2014.329

Self-destabilizing loop observed in a jetting-to-dripping transition

Akira Umemura† **and Jun Osaka**

Department of Aerospace Engineering, Nagoya University, Nagoya 464-8603, Japan

(Received 16 October 2013; revised 22 May 2014; accepted 5 June 2014;
first published online 2 July 2014)

It is well known that water slowly issued vertically downward exhibits a hysteresis phenomenon. A jetting-to-dripping transition appearing upon a stepwise decrease in jet issue speed was used to identify the origin of the Plateau–Rayleigh unstable wave elements which disintegrate the jetting liquid. In the present laboratory experiment using a stainless steel nozzle of inner radius 1 mm and length 30 mm, the transition occurred at a dimensionless jet issue speed of $\sqrt{\rho U^2 a_0/\sigma} = 0.8$, where ρ and σ respectively denote the density and surface tension coefficient of the liquid issued at the speed U from the nozzle of radius a_0. The jet length gradually shortened with an oscillation of considerably large amplitude and period. High-speed camera images show that this oscillation is caused by tip contraction capillary wave (TCCW) elements which are elongated by the gravitationally accelerating jet flow and become Plateau–Rayleigh unstable wave elements. The jet length increases while the jet tip experiences end-pinching and radiates TCCW elements upstream. Only those TCCW elements destabilized at appropriate locations can grow sufficiently to shorten the jet. Since the unstable wave elements produced nearer the nozzle exit have much smaller amplitude at the jet tip, the end-pinching becomes effective. Thus, these processes are repeatable and constitute a self-destabilizing loop. The observed jetting-to-dripping transition has nothing to do with the random nozzle disturbances which were believed to be the origin of the Plateau–Rayleigh unstable wave in conventional instability theories. It is also different from the feature conjectured from current absolute/convective instability analysis. The underling physics of the self-destabilizing loop are explored in detail by numerical simulations based on a one-dimensional model.

Key words: capillary waves, instability, waves/free-surface flows

1. Introduction

Numerous studies have been conducted on liquid jet instabilities, as described in the comprehensive reviews of Chandrasekhar (1961), McCarthy & Molloy (1974), Lin & Reitz (1998), Lin (2003) and Eggers & Villermaux (2008). In the present paper, we revisit the basic concepts underlining the linear instability analyses employed in these studies. Conventional linear stability analyses assume the presence of random

† Email address for correspondence: akira@nuae.nagoya-u.ac.jp

https://doi.org/10.1017/jfm.2014.329 Published online by Cambridge University Press

disturbances of the issued liquid (external disturbances) which naturally excite a convectively unstable wave. However, to the best of the authors' knowledge there is no literature proving the validity of this hypothesis, either theoretically or experimentally. Then, we cannot ignore a possibility that, if an observed convectively unstable wave is produced by an 'unknown' deterministic mechanism operating within the liquid jet region, its excitation might be attributed to nozzle flow noises so long as the deterministic mechanism is veiled.

To address such fundamental issues, it is best to start by considering the stability problem of the simplest liquid jet. Therefore, in the present paper, we confine ourselves to low-speed water jets issuing into room air. Here 'low-speed' means that the liquid jet is issued in a laminar flow state and the relative velocity between the liquid and gas phases does not contribute significantly to the jet instability. 'Water' means that the inviscid incompressible liquid approximation can be applied in the linear stability analysis. Of course, in real liquid jets there are various complicating factors involved, which have been intensively investigated, in particular, viscosity (Weber 1931; Nelson, Power & Seffert 1995; Tomotika 1955; Power & Goldstein 1997; Gañán-Calvo 1998; Anna, Bontoux & Stone 2003; Guillot *et al.* 2007), gas density (Leroux, Dumouchel & Ledoux 1997), injector shape (Grant & Middleman 1966; Meister & Scheele 1967; Phinney & Humphries 1973; Sterling & Sleicher 1975; Karasawa *et al.* 1992; Blasisot & Adeline 2003), nonlinear dynamics (Eggers & Dupont 1994; Ashgriz & Mashayek 1995; Eggers 1997), gaseous force (Bachelor 1958; Fenn & Middleman 1969; Lasheras & Hopfinger 2000; Yecko, Zaleski & Fullana 2002; Gordillo & Pérez-Saborid 2005; Yecko & Zaleski 2005; Pan & Suga 2006; Shinjo & Umemura 2010, 2011) velocity profile (Leib & Goldstein 1986; Reitz & Bracco 1986; Debler & Yu 1988; Ibrahim & Marshal 2000) and turbulence (Mayer 1961; Wu, Miranda & Faeth 1995; Marmottan & Villermaux 2004; Gorokhovski & Hermmann 2008).

1.1. *Low-speed jet in microgravity*

While laboratory experiments use gravity to create a straight liquid jet by issuing the liquid vertically downward, early linear stability analyses neglected gravity effects for simplicity. In this microgravity case, the baseline jet flow (free from surface tension effects) is a semi-infinitely long liquid column with a uniform average axial velocity and radius. The pioneering works by Plateau (1873) and Rayleigh (1878) paved the road for temporal evolution analysis of liquid jet instability. For a plug flow jet, temporal evolution analysis predicts a breakup length proportional to the jet speed, under the assumption that the issued liquid always contains a disturbance corresponding to the most unstable wave component. This predicted behaviour appears to be consistent with laboratory experiment observations. The linear increase in breakup length with jet issue speed, observed in low-speed jet issue conditions, is commonly called the Rayleigh regime (Lin & Reitz 1998).

When the same convectively unstable wave element is produced at the nozzle exit periodically, its spatial evolution becomes periodic in time. This is the basic idea of spatial evolution analysis. Keller, Ubinow & Tu (1973) showed that the spatial evolution solution coinciding with the Plateau–Rayleigh unstable wave is obtained in an infinitely large jet speed limit among an infinite number of spatially developing wave solutions. The effect of the cross-sectional velocity profile was investigated by Leib & Goldstein (1986) in their spatiotemporal evolution analysis to predict the emergence of absolute instability at low jet speeds. The experimental validation of

https://doi.org/10.1017/jfm.2014.329 Published online by Cambridge University Press

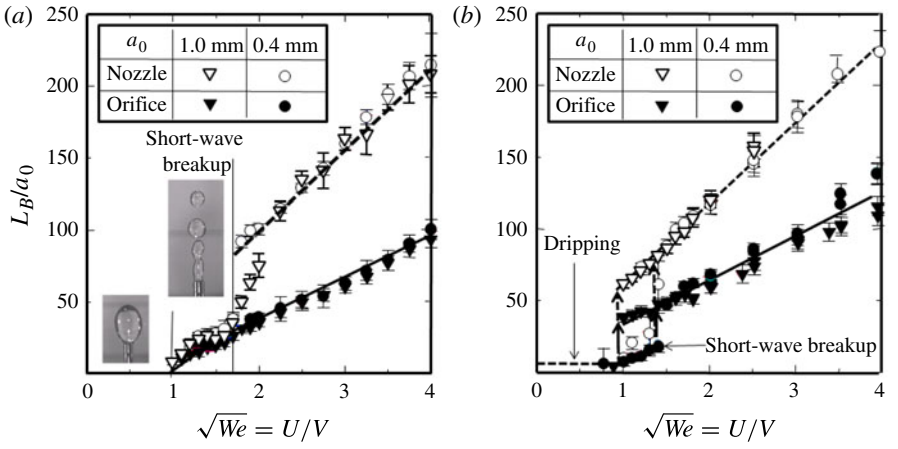


FIGURE 1. Dependence of steady breakup length on jet issue speed: (*a*) in microgravity; (*b*) under normal gravity. In each 4 s duration experiment, water is issued into atmosphere from a nozzle or orifice of radius a_0 at a constant speed U. Here, L_B denotes the average breakup distance from the injector exit. The deviation of each plot is indicated with a bar. Here, $V = \sqrt{\sigma/\rho a_0}$ is the jet tip recession speed. In the microgravity experiments, dropping does not take place at $U/V < 1$. At $1 < U/V < 1.6$, short-wave breakup is dominant. This range is included in the range for which absolute instability is predicted to appear. Other breakups are due to long-wave breakup caused by the growth of Plateau–Rayleigh unstable wave.

this prediction was reported by Monkewitz *et al.* (1988), Vihinen, Honohan & Lin (1997) and O'Donnell, Chen & Lin (2001). However, we should note that these linear stability analyses do not take into account the presence of the jet tip. Any unstable jet must have a tip somewhere at a finite distance from the injector. The surface tension acting along the generating lines of a liquid jet tends to contract the jet tip. As a result, the jet tip has a recession speed (Taylor 1959) and radiates a dispersive capillary wave upstream (Umemura 2011). The recessing jet tip accumulates liquid and takes a bulbous form with a necked portion connecting to the upstream liquid column. A breakup caused by a local instability at this necked portion is called 'end-pinching' (Taylor 1959; Stone & Leal 1989; Schulkes 1996; Gordillo & Gekle 2010). Since the necked portion must have an upstream propagation speed for end-pinching to take place, Umemura (2011) termed this local instability 'short-wave breakup' in order to distinguish it from the 'long-wave breakup' caused by a Plateau–Rayleigh unstable wave. Since a jet tip is newly produced upon every breakup, the short-wave breakup is repeatable due to its own local instability. The short-wave breakup process partially exhibits an absolute instability behaviour.

Figure 1(*a*) shows the results of our recent microgravity experiments (using the same apparatus as described in § 2.1) in parabolic flights, in which liquid issued at a speed U from a nozzle or orifice tends to form a uniform, circular cylindrical liquid column as assumed in the above-mentioned analyses. The jet tip recession speed is $V = \sqrt{\sigma/\rho a_0}$ where σ, ρ and a_0 denote the surface tension coefficient, liquid density and jet radius, respectively. Therefore, when the ratio of the jet issue speed, U to jet tip recession speed V, which is the square root of the Weber number $\sqrt{We} = U/V$, is less than unity, no steady liquid jet column is formed. The issued liquid simply formed a growing bulb on the injector exit over the course of the 4 s

https://doi.org/10.1017/jfm.2014.329 Published online by Cambridge University Press

experiment; hence, the breakup length is regarded as being zero in the figure. As $\sqrt{We}$ is increased from unity, the average breakup length increases from zero. In the range $1 < \sqrt{We} < 1.6$, short-wave breakup takes place dominantly. The average breakup length does not depend on the issued liquid velocity profile. At $\sqrt{We} > 1.6$, the jet exhibits long-wave breakup. The average breakup length is different between the orifice and nozzle jets, but the breakup wavelength is consistent with the value predicted by the Plateau–Rayleigh theory. If a jet portion is absolutely unstable, the disturbance introduced at that portion is likely to grow with time. In microgravity, this prediction should apply to any place along the orifice jet in a plug flow state. As can be seen from the microgravity experiment results in the range $1 < \sqrt{We} < 1.6$, the surface deformation near the injector exit remains small during the experiment. This discrepancy is not surprising. A finite length of continuous jet with its tip downstream and a constraint at the injector exit upstream may produce a different behaviour from what is predicted by the current absolute analysis which does not account for these boundary conditions but considers only the asymptotic behaviour after a long elapsed time. The microgravity experiment results suggest that consideration of the role played by the jet tip is important for characterizing the real jet instability.

1.2. *Low-speed jet under normal gravity*

Figure 1(*b*) shows our laboratory experiment results under normal gravity using the same injectors as for the microgravity experiments. The results are consistent with those of other experiments that use a different injection system (Hiroyasu, Arai & Shimizu 1991; Amagai 2000). At large jet issue speeds, both normal- and micro-gravity jets exhibit similar breakup length behaviours. The gravitational jet acceleration effect becomes significant at low jet speeds. It is known that the breakup length exhibits hysteresis in a certain low-jet-issue-speed range. When the jet issue speed U is increased stepwise from a small value, dripping is first observed. At a certain value (U_1) of jet issue speed, the average breakup length jumps to a large value by a transition to a jetting state. Further increases in jet issue speed lengthen the breakup length in proportion to the jet issue speed. When the jet issue speed is decreased stepwise from a jetting state, the breakup length shortens, tracing back the same dependence on jet issue speed until a certain value (U_2 ($<U_1$)) of jet issue speed, at which the jetting state transitions to dripping. The hysteresis range $U_2 < U < U_1$ depends on the Bond number Bo.

The breakup characteristics in the steady jetting ($U > U_1$) and dripping ($U < U_2$) states have been investigated in the past. A concise historical review of dripping studies was made by Clanet & Lasheras (1999). It is known that dripping is periodic at lower jet issue speeds and chaotic (Coullet, Mahadevan & Riera 2005) at higher jet issue speeds. The critical jet issue speed V_J, at which the transition from dripping to jetting takes place, can be expressed as $V_J = K(B_0)\sqrt{\sigma/\rho a_0}$ (Smith & Moss 1917; Tyler & Richardson 1925; Tyler & Watkin 1932). Relatively recently attention has been directed to the transition mechanisms between dripping and jetting. Clanet & Lasheras (1999) proposed a one-dimensional model for the dripping-to-jetting transition, in which Taylor's (1959) model for a recessing liquid edge is extended to describe the behaviour of a pendant inviscid liquid. The critical Weber number expression derived as the condition for the short-wave breakup location to begin to move downward is in good agreement with experiments. On the other hand, the jetting-to-dripping transition mechanism has not been explored fully. Lin & Lian (1989) and Monkewitz (1990) conjectured that the jetting-to-dripping transition is

https://doi.org/10.1017/jfm.2014.329 Published online by Cambridge University Press

related to the global absolute instability. Le Dizes (1997) proposed that an orifice jet becomes absolutely unstable at the orifice exit when the jet issue speed is decreased to the critical value ($We = \pi$) predicted by Leib & Goldstein (1986) and that this causes the jetting-to-dripping transition. However, even if the jetting-to-dripping transition is observed in an experiment, we cannot conclude that the transition is caused by the proposed mechanism and not by other mechanisms. Therefore, we need a more detailed study on the jetting-to-dripping transition mechanism.

1.3. *Purpose of the present study*

It is clear that the jetting-to-dripping transition mechanism cannot be uncovered without a deeper understanding of the origin of convectively unstable waves. Before settling in the dripping state, the jet must be shortened by the Plateau–Rayleigh unstable wave. Therefore, the traditional instability theories, which presume that nozzle flow noises are the origin of the Plateau–Rayleigh unstable wave and predict the steady breakup length determined by the jet issue speed, is encountered with a serious difficulty, because the jet issue speed is fixed and the baseline jet flow is unchanged during the transition. The random disturbances must change their constituents (wavenumber and amplitude) in response to the reduced breakup distance. This is inconsistent with the conventional selection concept and causality. On the other hand, dripping is obviously associated with jet tip contraction. Therefore, a consideration of the jet tip behaviour is necessary to bridge the jetting and dripping states, and a theory which can account for both short-wave and long-wave breakups is needed to describe the jetting-to-dripping transition mechanism.

Based on microgravity experiments, Umemura (2011) considered the origin of the Plateau–Rayleigh unstable wave and proposed a self-destabilizing mechanism to determine the steady breakup length. The proposal claims that the unstable wave disintegrating the jet is produced by past events occurring in the jet region. More specifically, dispersive capillary wave elements, produced by a downstream nonlinear process such as unstable wave growth or contraction of a jet tip that was newly produced by a short-wave breakup, may become unstable wave elements due to elongation caused by nozzle exit reflection (Umemura 2011) or accelerating jet stretching (Umemura *et al.* 2011). Therefore, this theory could describe the hysteresis phenomena as well. However, the existence of such a self-destabilizing loop has not yet been confirmed experimentally for the following reasons. Experimentally, it is relatively easy to trace the behaviour of an amplified unstable wave element, but it is difficult to capture the process of a capillary wave element becoming an unstable wave element, because its surface deformation is very small (note that the smallness of capillary wave amplitude does not constrain the existence of capillary wave). Furthermore, in a steady breakup state, it is difficult to isolate a particular sequence of capillary wave elements, because other overlapping capillary waves mask it.

Interestingly, exploring the jetting-to-dripping transition process offers the opportunity to detect an isolated tip contraction capillary wave (TCCW). In fact, if the self-destabilizing mechanism is correct, the jet near the nozzle exit is in an almost undisturbed state until the transition onsets, because the jet tip is located far from the nozzle exit. In the shortening jet length process, we will be able to observe a dispersive capillary wave propagating into the newly issued liquid column becoming an unstable wave, without serious interference with overlapping waves generated in the past. Therefore, the present study has the two purposes of (i) experimentally validating the presence of a self-destabilizing mechanism and (ii) revealing the

https://doi.org/10.1017/jfm.2014.329 Published online by Cambridge University Press

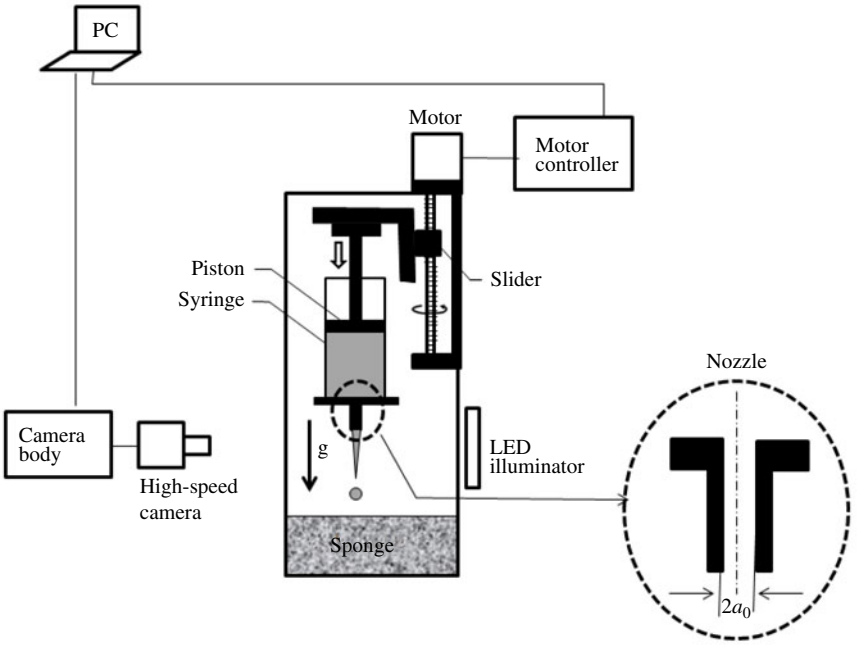


FIGURE 2. Experimental system.

jetting-to-dripping transition mechanism. In this study we report the experimental results of extracting a self-destabilizing loop in our recent laboratory experiments and detail the underlying physics by theoretically analyzing the experimental results and conducting a one-dimensional model numerical calculation mimicking the transition. The present paper is the first study experimentally documenting the real dispersive capillary wave behaviours to be considered in linear stability analysis.

The structure of the present paper is as follows. Section 2 presents the results from our hysteresis experiment. In the jetting-to-dripping transition of a nozzle jet, it is observed that the jet length gradually shortens, repeating a cyclic jet length oscillation which consists of a short-wave breakup phase lengthening the jet and a long-wave breakup phase shortening the jet. A pattern of bulging and necked portions obtained for one cycle of jet length oscillation clearly shows that the dispersive capillary wave elements radiated from the jet tip are elongated in the gravitationally accelerating jet and become Plateau–Rayleigh unstable wave elements. Section 3 presents one-dimensional model numerical calculations which were conducted to explore the self-destabilizing loop observed in the experiments and to detail the underlying physics of the jetting-to-dripping transition. Section 4 summarizes the findings of the present study.

2. Hysteresis experiment under normal gravity

2.1. *Experimental method*

Figure 2 illustrates the setup used in the present laboratory experiments. Pure water, contained in a syringe of inner diameter 35.9 mm is pushed out by a piston, through a straight stainless steel nozzle of inner diameter $2a_0 = 2$ mm, outer diameter 3 mm and length 30 mm, which is attached to the flat end of the syringe as shown by

https://doi.org/10.1017/jfm.2014.329 Published online by Cambridge University Press

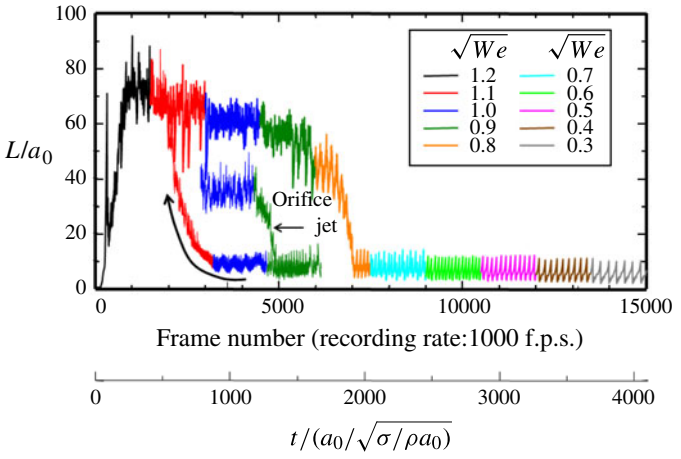


FIGURE 3. Jet tip location history.

the magnified view. The syringe is fixed vertically in space, and the water is issued downward. A threaded rod is rotated by an AC motor (Oriental Motor Co.). A ball screw mechanism transforms the rot rotation to the linear motion of the slider rigidly connected to the piston. The relationship between the motor revolution speed and water flow rate Q is calibrated by measuring the volume of water issued from the nozzle over time. The instantaneous jet issue speed U, which is obtained by dividing Q by πa_0^2, is controlled by the programmed motor controller. The surface deformation of the water jet, backlit by a planar light source (an LED array covered with a holographic diffuser), is photographed with a high-speed CCD camera (Fotron Co., FASTCAM-MAX) at a frame rate of 1000 f.p.s. with a shutter speed of 15 000 s^{-1}. The size of the captured images is 1024 pixels × 128 pixels. The motor revolution speed over time is recorded.

2.2. *Jet tip location history*

The water jet tip is defined as the downstream end of a continuous water column issued from the nozzle. Its instantaneous distance $L(t)$ from the nozzle exit $x = 0$ was measured from the high-speed images. When the jet disintegrates at a location upstream of the jet tip, $L(t)$ is discontinuously shortened to the breakup location at that instant. Otherwise, $L(t)$ changes with time continuously. Figure 3 shows the history of the dimensionless jet tip location L/a_0 obtained in an experiment run, in which the dimensionless jet issue speed $\sqrt{We} = U/\sqrt{\sigma/\rho a_0}$ was decreased stepwise by decrements of 0.1 from $\sqrt{We} = 1.2$ to 0.3. The duration of each jet issue speed step was 1.5 s, which is sufficiently longer than the time required for a jet element to travel the distance L. The transition from jetting to dripping was observed at $\sqrt{We} = 0.8$. The experiment was repeated three times to ensure repeatability. We conducted a reverse experiment, in which the jet issue speed was increased stepwise from $\sqrt{We} = 0.3$ to 1.2. Its result is also plotted in figure 3, which should be read from right to left as indicated by the arrowed line. To avoid overlapping of the plots, the data for $\sqrt{We} > 0.7$ from the reverse experiment are not plotted, although they coincide with the dripping behaviour in the decreasing jet issue speed experiments. The jet tip location history, obtained when water was issued from an orifice hole of

https://doi.org/10.1017/jfm.2014.329 Published online by Cambridge University Press

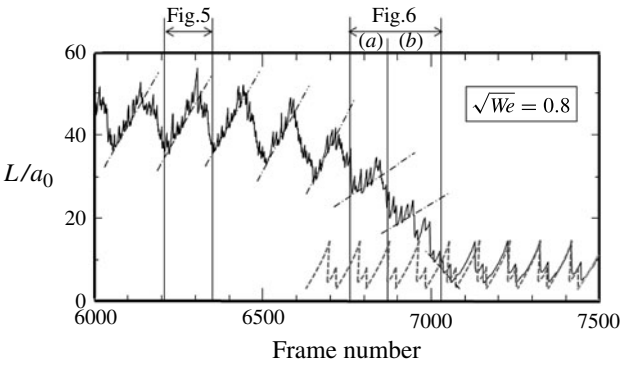


FIGURE 4. Jet tip location history at $\sqrt{We} = 0.8$. The grey dotted line denotes the jet tip location history in the dripping state of Clanet & Lasheras (1999) experiment (under the same liquid issue condition) for comparison. The dotted–dashed lines pass through the short-wave breakup locations in a least-squares method sense. Their slopes agree fairly well with $\mathrm{d}L/\mathrm{d}t = 1.375\sqrt{\sigma/\rho a_B} - u_B$, which expresses the breakup location movement caused by repetition of short-wave breakup (Umemura *et al.* 2011), where the local jet velocity u_B and radius a_B of baseline jet flow are evaluated at the initial short-wave breakup location. The initial three dotted–dashed lines have almost the same slope. The slope decreases for later lines. When the jet length becomes comparable with the maximum jet length in the dripping state, the slope becomes negative.

radius $a_0 = 0.1$ mm, is also partially plotted in the figure to show the difference from the jetting-to-dripping transition of the nozzle jet.

As seen from figure 3, the jet length exhibits hysteresis behaviour. At low jet issue speeds, dripping occurs steadily while jetting occurs steadily at high jet issue speeds. In the present experimental conditions, the dripping-to-jetting transition occurs at $\sqrt{We} = 1.1$ while the jetting-to-dripping transition occurs at $\sqrt{We} = 0.8$. As stated in § 1, the dripping-to-jetting transition mechanism is known. However, the jetting-to-dripping transition mechanism has not been explored fully. In the following, we are only interested in the decreasing jet issue speed case. When the jet issue speed is abruptly decreased to another fixed value, a jet element between the downstream higher-speed and upstream lower-speed columns is stretched. The resulting necked portion destabilizes and breaks up. If such a breakup happens within a certain distance from the nozzle exit, the jet length is rapidly shortened by repeated end-pinching. For a small decrement of jet issue speed, this type of breakup near the nozzle exit can be avoided. In the present experiment, the jet length is gradually shortened to bring about a transition to dripping. This is what we expected.

2.3. *Transition from jetting to dripping*

Figure 4 shows the jet tip location history during the jet issue speed step $\sqrt{We} = 0.8$ in figure 3. The graph before settling into the dripping state may be decomposed into the following three components: (*a*) a short period of saw-tooth-like change, which expresses the jet tip displacement between successive breakups. We may consider a smoothed jet length curve which passes all breakup locations in a least squares method sense. This curve characterizes the observed jetting-to-dripping transition. It consists of (*b*) a long-period (approximately 0.143 s) damped oscillation with a large

https://doi.org/10.1017/jfm.2014.329 Published online by Cambridge University Press

initial amplitude (about $15a_0$) (called a 'smoothed jet length oscillation') and (*c*) a monotonically decreasing average jet length ('transition curve'), which decreases gradually during the first five cycles of (*b*) and then rapidly settles to a constant value of dripping. The jet breakup occurs approximately 10 times during the period of (*b*). Therefore, even if (*b*) is caused by the oscillation of the jet issue speed, this cannot be a cause for (*a*). In the present paper, we would like to show that (*a*) causes (*b*) which results in (*c*) and that any possible jet issue speed variation, if there, is not associated with this transition. To do this, we need to eliminate the possibility that (*b*) is caused by jet issue speed oscillation.

In the present injection system, it is difficult to measure the instantaneous flow rate of the issuing water. The instantaneous motor revolution speed was monitored, which suggest a possible $\sqrt{We}$ oscillation of 0.05 s and amplitude 0.007 at most. This period is shorter than the typical period of (*b*) and longer than the typical period of (*a*). However, we cannot determine exactly the effects of the frictional force between the piston and syringe wall and the elastic deformation of the syringe, although they tend to suppress the motor's oscillation effect. Therefore, to ensure that (*b*) is not due to any jet issue speed fluctuation we searched related literature for reports of other experiments using different injection systems. Note that the jet issue condition is nominally fixed at $\sqrt{We} = 0.8$ for the time period under consideration, in both the initial jetting state and the final dripping state. Unfortunately, there is no literature reporting the transient jet tip location behaviour in the jetting state, although Clanet & Lasheras (1999) reported the water column tip history in the dripping state. In their experiments, water at room temperature is pushed out under a constant pressure into a straight stainless steel nozzle of inner diameter 1.6 mm and length-to-diameter ratio >50 through a regulator and a flow meter. Their experimental result is shown by the grey line in figure 4 for comparison. The behaviour is almost identical with that of the present experiment after the transition to dripping. Therefore, in the following, our experimental results will be interpreted under the recognition that the instantaneous jet issue speed is fixed at the constant value $\sqrt{We} = 0.8$ during the jetting-to-dripping transition process.

Figures 5 and 6 show a sequence of high-speed images at the initial and final stages indicated in figure 4, respectively. Only half of the view of the jet is shown, utilizing the fact that the jet is axisymmetric. The time spans of figures 5 and 6(*a*) are selected so as to be suitable for characterizing a cycle of the smoothed jet length oscillation. The first and last frames correspond to the instant when the smoothed jet length oscillation takes a minimum value. In all high-speed images, the size of nozzle radius a_0 is resolved with approximately 10 pixels. The jet surface deformation, which has an amplitude comparable with or smaller than one pixel, cannot be resolved. Nevertheless, the deformed surface refracts the back light and makes the jet image brighter at the bulging portions and darker at the necked portions. By virtue of this brightness pattern along the jet, we can detect even very small surface deformations in the high-speed images and trace their movements and wavelength changes. The essential features of the jet deformation near the jet tip are common between figures 5 and 6(*a*). It is found that a cycle of the smoothed jet length oscillation consists of two phases: (i) an increasing jet length phase, in which no appreciable growth of a Plateau–Rayleigh unstable wave element is observed while a dispersive capillary wave is radiated from the newly produced jet tip upon every short-wave breakup; (ii) a decreasing jet length phase, in which appreciably amplified Plateau–Rayleigh unstable wave elements disintegrate and shorten the jet. Since the Plateau–Rayleigh unstable wave elements are produced from the dispersive capillary wave radiated by the jet tip

https://doi.org/10.1017/jfm.2014.329 Published online by Cambridge University Press

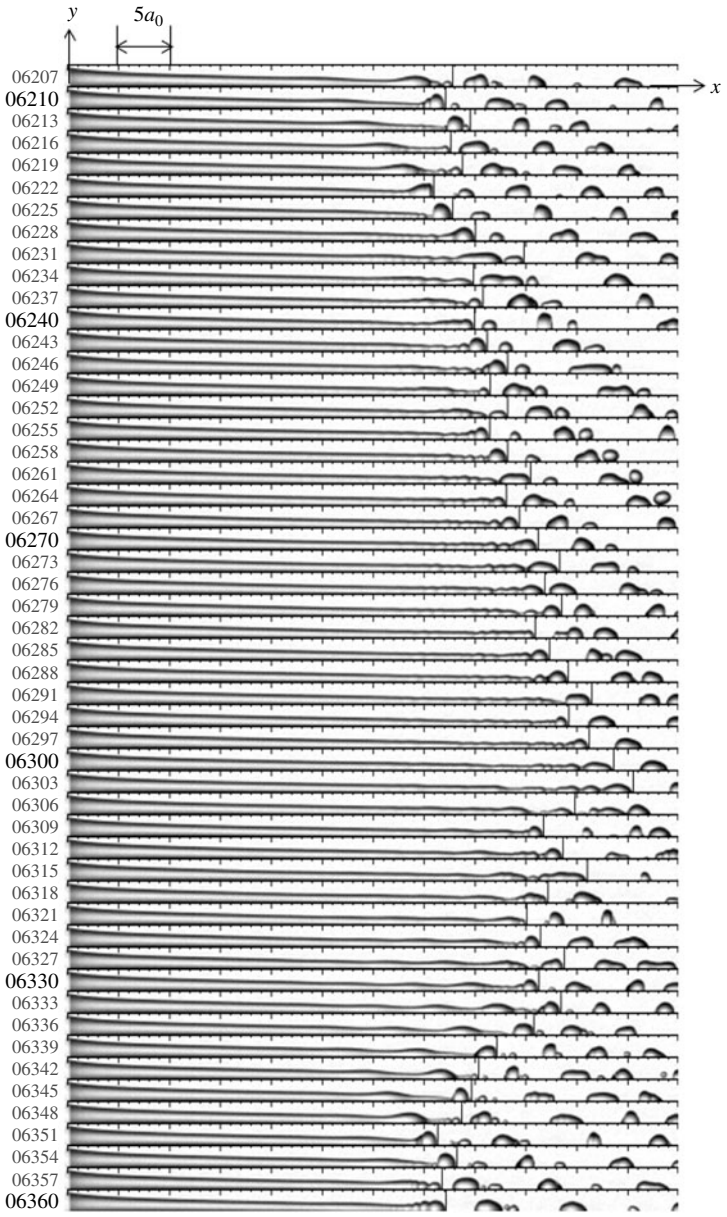


FIGURE 5. High-speed images at an initial stage of jetting-to-dripping transition. Each image is presented every third frames. By axisymmetry, only a half view of the jet is shown. The x-coordinate is measured from the nozzle exit along the jet centreline. The origin of y-coordinate is taken on the jet centre line.

contraction, this cycle is self-sustained. The underlying physics will be detailed in §§ 3 and 2.4.

The brightness pattern was used to investigate the jet deformation structure near the final stage of the jetting-to-dripping transition, when the jet is shortened and deforms with a relatively larger jet radius. The jet region of $x/a_0 < 25$, where

https://doi.org/10.1017/jfm.2014.329 Published online by Cambridge University Press

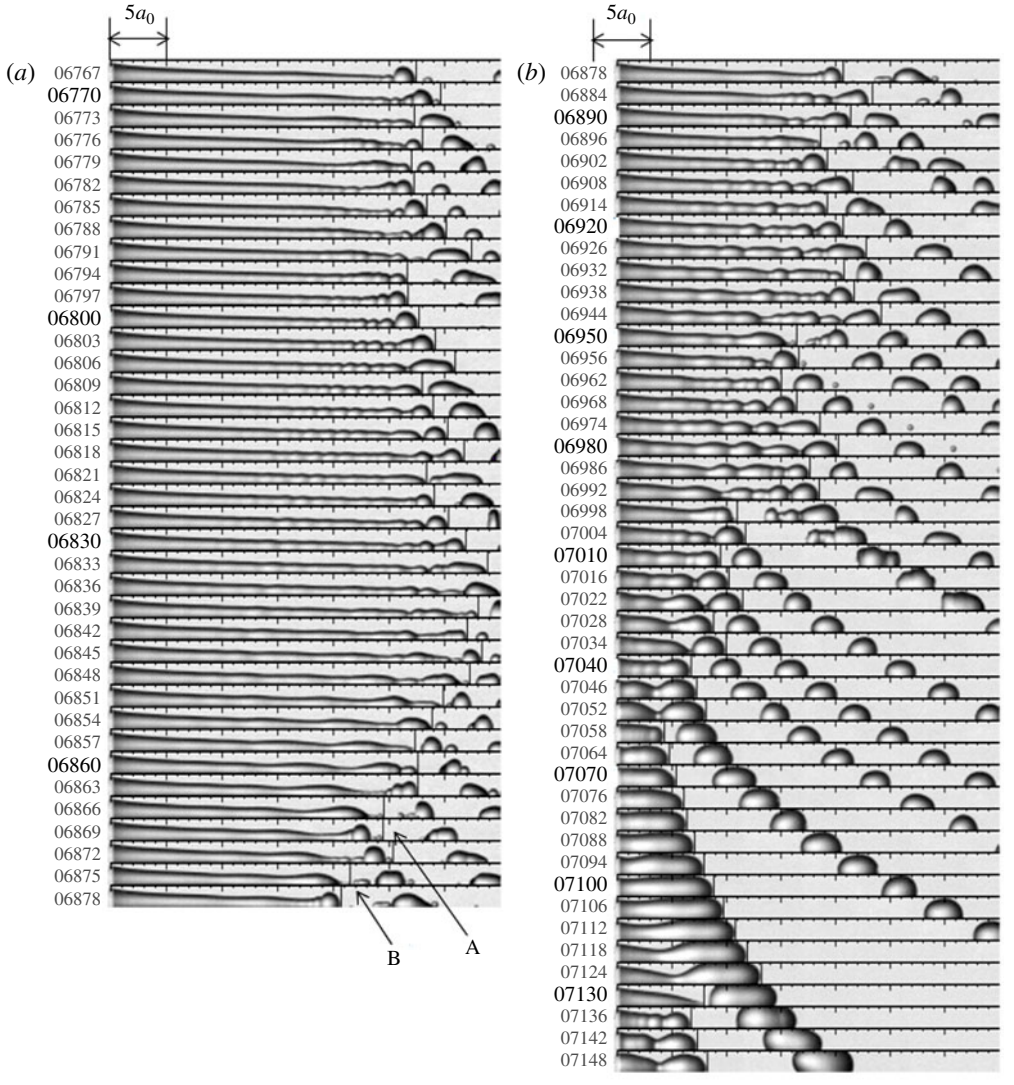


FIGURE 6. High-speed images at a final stage of jetting-to-dripping transition. Each image is presented every three (*a*) or six (*b*) frames.

appreciable surface deformation is observed in figure 6, is in an almost undisturbed state in figure 5. We subtracted a time-averaged image (brightness distribution $I_0(x, y)$) of figure 5 from each image (brightness distribution $I(t, x, y)$) during frame numbers 6800–7000 of figure 6. The resulting images are considered to be a good representation of the jet deformations. We integrated the brightness difference across the jet at each distance x from the nozzle exit:

$$\Delta I(t, x) = \int |I\,(t, x, y) - I_0(x, y)|\ \mathrm{d}y. \tag{2.1}$$

The variation of ΔI with x expresses the degree of jet surface deformation. The bright and dark portions correspond to the bulging and necked portions of the jet,

https://doi.org/10.1017/jfm.2014.329 Published online by Cambridge University Press

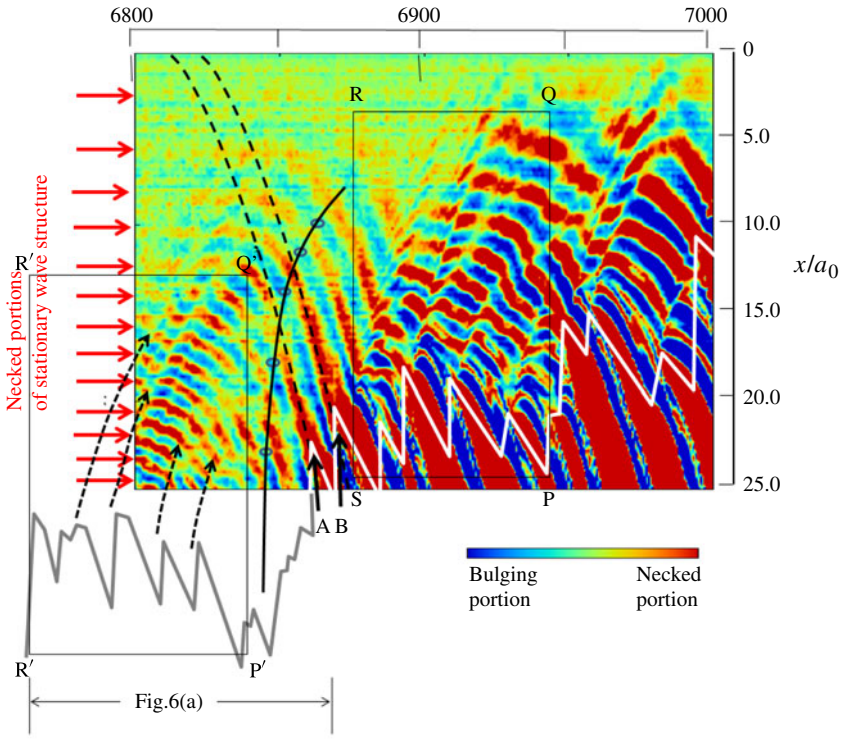


FIGURE 7. Jet deformation pattern. The striped pattern of bulging and necked portions during frame numbers 6800–6900 illustrates the behaviours of the dispersive capillary wave elements radiated by the contractions of the newly produced jet tip upon a series of short-wave breakups during frame numbers 6767–6842. The white and grey zigzag lines denote the jet tip location history. The regular temporal brightness variation recognizable near the nozzle exit is due to the use of alternative current LED illumination. The black dashed line denotes the trajectory of a jet element. The open circles connected by the black solid line denote the locations where a propagative TCCW element changes to an unstable wave element. The red arrowed lines indicate the centres of necked portions of the stationary wave explained in § 3.2.

respectively. Figure 7 shows ΔI (t, x) as a colour map, illustrating a clear stripe pattern of bulging (blue) and necked (red) portions produced by dispersive capillary waves. The high-speed images in figure 6(*a*) correspond to the range of frame numbers 6800–6900 in figure 7. As explained in § 2.4, the stripe pattern observed in this period captures the self-destabilizing process experienced by the jet TCCW elements. No appreciable variations triggering the striped pattern can be recognized near the nozzle exit. Therefore, the nozzle flow noise, if present, has nothing to do with the observed transition.

As shown in figure 3, we conducted the same experiment for an orifice jet and observed similar hysteresis behaviour. The orifice jet is more suitable for theoretical consideration, in that the issued jet element has a nearly uniform velocity profile. However, it was difficult to isolate the behaviour of dispersive capillary wave as a clear stripe pattern for the following reasons. (i) Wetting. The orifice was made by drilling a thin (0.4 mm) flat plate fitted to the syringe end. The water flowing out of the hole wets the outer plate surface to a considerable extent at low jet issue speeds.

https://doi.org/10.1017/jfm.2014.329 Published online by Cambridge University Press

As a result, the wetting effect cannot be ignored. (ii) Short jet length. As shown in figure 1, the average breakup length of the orifice jet is shorter than that of the nozzle jet. Therefore, the jetting-to-dripping transition starts from a short jet length, and we cannot get a reference high-speed image with an undisturbed jet portion, which is necessary in the calculation of (2.1) to obtain a clear stripe pattern. This is possible only when the initial jet is long enough and has a considerable length of undisturbed jet portion. In the jetting-to-dripping transition of the orifice jet, the whole jet portion is disturbed from the beginning.

2.4. *Identification of the self-destabilizing loop*

The nonlinear processes (jet tip recession followed by short-wave breakup and breakup by the growth of a Plateau–Rayleigh unstable wave) take place in a restricted region near the jet tip. Upstream of this region, the jet surface deformation is small enough to be treated in the framework of linear theory. Using simple theory, figures 6 and 7 can be physically interpreted as described below. More detailed analyses are given in § 3.

From free fall dynamics, the steady laminar jet flow is expressed as

$$\frac{u}{U} = \left(\frac{a_0}{a}\right)^2 = \sqrt{1 + \frac{2Bo}{We}\frac{x}{a_0}}, \tag{2.2}$$

where a and u denote the local jet radius and average axial velocity along the centreline coordinate x measured from the nozzle exit. For our experimental conditions, the Bond number is $Bo = \rho g a_0^2/\sigma = 0.136$ and the Weber number is $We = \rho U^2 a_0/\sigma = 0.64$. It is found that the local Weber number $\rho u^2 a/\sigma$ takes a considerably larger value than unity at large distances from the nozzle. Once the effect of surface tension is introduced, no steady jet flow realizes from the instant of liquid issue start. Nevertheless, (2.2) is useful for considering the behaviour of small-amplitude capillary perturbation waves excited in a temporally varying length of liquid jet (upstream of the breakup location). The dispersion relation, derived from an inviscid local linear stability analysis of the baseline flow (2.2), yields a neutral (propagative) wave or an unstable wave depending on the value of local wavelength, $\lambda = 2\pi/k$, according to the complex phase velocity expression:

$$c_r = u \pm v, \quad v = \sqrt{\frac{\sigma}{2\rho a}\left\{(ka)^2 - 1\right\}}. \tag{2.3}$$

In the present problem, it is important to note that a propagative wave element may change to an unstable wave element through wavelength elongation due to the accelerating jet flow (2.2).

In a cycle of smoothed jet length oscillation in figure 6(*a*), we can distinguish two phases.

2.4.1. *Short-wave breakup phase lengthening the jet*

Frame 6794 is the instant when the smoothed jet length minimizes. The jet surface appears smooth except near the jet tip ($x = x_B$) which contracts due to surface tension and causes a short-wave breakup (end-pinching) as well as an upstream radiation of dispersive capillary wave (termed a TCCW). In this process, part of the surface energy released by the tip contraction is transferred in the upstream direction in the form of

https://doi.org/10.1017/jfm.2014.329 Published online by Cambridge University Press

a capillary wave (Umemura 2011). Similar short-wave breakups subsequently occur several times. Since the jet tip contraction speed $V = \sqrt{\sigma/\rho a(x = x_B)}$ (Taylor 1959; Schulkes 1996; Umemura 2011) is smaller than the local jet speed $u(x = x_B)$, the jet length increases in this phase.

A primitive image of each TCCW is given by a dispersive capillary wave produced by an impulsive forcing at a newly produced jet tip. It consists of a series of wave elements that have shorter wavelength (thereby larger upstream propagating speed) and smaller amplitude the farther they are from the forcing location. A short-wave element with $(-v) > u$ moves in the upstream direction until the reduced $(-v)$ becomes equal to u.

The accelerating jet flow enhances the TCCW element elongation. This effect is clearly observed in figure 6(*a*) for TCCW elements located near the jet tip, which have rather large surface deformation amplitudes. For example, the three TCCW elements near the jet tip in frame 6800 have decreasing wavelengths in the upstream direction, but the degree of wavelength reduction is small compared with that in the non-stretching jet case.

A TCCW element whose upstream propagation speed $(-v)$ momentarily matches u (termed a 'stationary wave element') does not remain at the same location. This is because the wave element is elongated when the upstream shorter element moves in the upstream direction and the downstream longer element moves in the downstream direction. The stationary wave element subsequently moves downward and continues to be elongated. This process is clearly captured as a series of parabolic-like red lines in figure 7. The locus of each upstream-moving short TCCW element is not captured as a continuously smooth red or blue line in the figure. Instead, it appears as a line distorting the parabolic-like red lines, which originates from the jet tip newly produced by a short-breakup as indicated by an arrowed dashed line. Upward- and downward-moving TCCW elements passing the same location have significantly different wavelengths. The upward-moving element produced later disturbs the downward-moving element produced earlier. This feature can be more clearly recognized on the stripe pattern formed by the next series of short-wave breakups after frame 6900, where it is also observed that the parabolic-like red lines becomes parallel to the jet tip trajectory as they approach the jet tip. This is because the elongated TCCWs near the jet tip tend to be steady with respect to the jet tip. The same behaviour appears in the short-wave breakup phase in other cycles. It is found from figure 6(*a*) that there are TCCW elements travelling up to $x/a_0 \sim 5$ in frame 6850, from which a Plateau–Rayleigh unstable wave element emerges later. Figure 7 shows the composite wave structure resulting from the TCCWs radiated by a series of short-wave breakups, which is characterized with the aid of numerical simulations in the next section. The increased distances of separation between neighbouring parabolic-like red lines show the continued elongation of the TCCW elements.

2.4.2. *Long-wave breakup phase shortening the jet*

It is apparent that the last two breakups (labelled A and B) in figure 6(*a*) are caused by the growth of Plateau–Rayleigh unstable wave elements. The two corresponding breakups in figure 7 are indicated by the same labels. In figure 7, the trajectory of a jet element (the solution of $\mathrm{d}x/\mathrm{d}t = u(x)$ subject to $x(t = 0) = 0$) passing either of points A or B is shown by two black dashed lines. The red stripes terminating at points A and B coincide with the two jet element trajectories up to a certain upstream location, ensuring that each Plateau–Rayleigh unstable wave element moves downward

https://doi.org/10.1017/jfm.2014.329 Published online by Cambridge University Press

at the local jet velocity $u(x)$ and its growth shortens the jet length. This implies that the accelerating jet flow lengthens the wavelength $\lambda = 2\pi/k$ of the unstable wave element according to $ku = \text{const.} = k_B u_B$, where the subscript B denotes evaluation at the breakup location x_B. Using this fact, we now trace back the Plateau–Rayleigh unstable wave element in the upstream direction. The location $x = x_N$, at which the unstable wave element becomes a neutral wave element, is the place of origin of the unstable wave element. This place is identifiable in figure 7 as where the red stripe deviates downward from the jet element trajectory. For example, the unstable wave element responsible for the breakup B is found to be produced at around $x/a_0 = 12$. Importantly, this downward deviation clearly indicates that the Plateau–Rayleigh unstable wave element is produced from a capillary wave element which has an upstream propagation speed $(-v) > 0$. In the present experiment, such a capillary wave element must be sustained by an energy transfer from downstream. Therefore, the propagative capillary wave element must be an elongated TCCW element. This process expresses the changing of a TCCW element to an unstable wave element in the accelerating jet flow. The main purpose of the present experiment was to observe this TCCW behaviour experimentally.

Measuring the distances of separation between the neighbouring parabolic-like red lines at each instant, we can determine the location, at which a propagative TCCW element becomes an unstable wave element in the figure. We defined this location as the mid-point x_N of the measured separation distance (equal to $2\pi a(x = x_N)$). The black solid line connects such multiple mid-points. This line indicates that the unstable wave elements are produced in a short time period after frame 6850, consistent with the observation in figure 6(*a*). The TCCW elements located on the left-hand side of the black solid line are propagative and transfer energy from downstream to upstream. The parabolic-like stripes (red online) on the right-hand side indicate the loci of Plateau–Rayleigh unstable wave elements. It is interesting to note that the black solid line originates from the jet tip and changes the dominant breakup mode from short-wave breakup to long-wave breakup. This implies that, once a Plateau–Rayleigh unstable wave element shortening the jet is produced from an elongated TCCW element, the energy supply from the jet tip ceases and the upstream TCCW elements gradually lose their upstream propagation speeds. The TCCW elements near the jet tip are affected first, followed by those further upstream in turn, resulting in the black solid line extending upward and gradually bending to the right.

In this connection, it is important to note the following. Figure 8 shows the long-wave breakup process of a Plateau–Rayleigh unstable wave element. The first image shows an instant immediately after the previous unstable wave element completes its long-wave breakup. In long-wave breakup, the necked portion becomes a thin liquid ligament connecting the downstream and upstream bulging portions. The newly produced jet tip bulb connected to the ligament behaves like a droplet undergoing Rayleigh oscillation and does not transfer significant energy upstream. Two breakups successively occur in the ligament portion, first at the downstream edge and then at the upstream edge. Thus, a large droplet and a satellite are produced from the downstream bulging portion and the ligament, respectively. The surface energy released by the tip recession of the ligament is small. Therefore, long-wave breakup does not produce any significant dispersive capillary waves propagating in the upstream direction. Since no TCCW is radiated while long-wave breakup is occurring, there must be a period during which no significant unstable wave elements are produced. This is the reason why the short-wave breakup phase and the long-wave breakup phase emerge alternatively in the smoothed jet length oscillation.

https://doi.org/10.1017/jfm.2014.329 Published online by Cambridge University Press

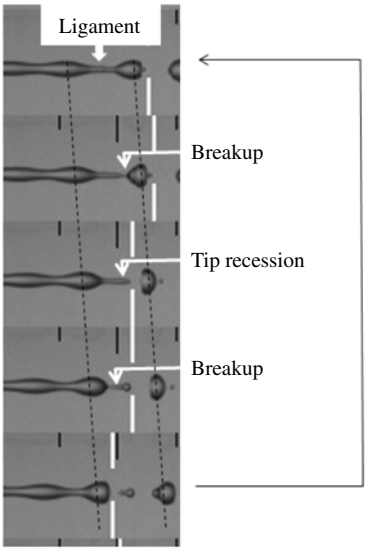


FIGURE 8. Long-wave breakup. The tip recession which occurs after the ligament is broken up does not result in any effective dispersive capillary waves transferring a significant amount of energy upstream.

Although an unstable wave element produced upstream has a small initial amplitude (equal to that of the destabilizing TCCW element), it can travel a rather long distance, maintaining a relatively large growth rate. As a result, it disintegrate the jet sufficiently upstream of the jet tip and shortens the jet by long-wave breakup. However, an unstable wave approaching the jet tip later must originate farther upstream with a much smaller initial amplitude. In addition, the larger jet stretching rate near the nozzle exit elongates its wavelength to a great degree exceeding the maximum growth rate wavelength. In fact, the breakup wavelengths at point A and B are about $7a_0$ and $7.8a_0$, respectively, which have already exceeded the maximum growth rate wavelength (nine times the local jet radius $a < a_0$). Thus, the subsequent unstable waves produced farther upstream are less and less amplified near the jet tip, which eventually results in a jet state similar to the initial state of the cycle. Then, the jet tip contraction again begins to operate effectively and TCCWs are radiated from the jet tip.

In figure 7, only the loci of TCCW elements with relatively large amplitudes can be observed. Therefore, it is obvious that the short and small-amplitude TCCW elements, which reach the nozzle exit and reflect, do not play an important role in the jetting-to-dripping transition.

As can be seen from figure 5, a similar striped pattern in a vicinity of the jet tip is observed for earlier cycles, although it becomes difficult to resolve other than parabolic-like lines due to the thinning jet. Nevertheless, the essential feature is the same. For example, the short-wave breakup phase stripe pattern in rectangle P′Q′R′S′ and those at earlier cycles are similar to that in rectangle PQRS. Only significant difference is that the parabolic-like lines have narrower spacing and larger slope as the jet tip velocity increases.

https://doi.org/10.1017/jfm.2014.329 Published online by Cambridge University Press

2.4.3. *Stationary wave structure produced by TCCWs*

The striped pattern of figure 7 is a visualization of the process in which TCCW elements change to Plateau–Rayleigh unstable wave elements in a gravitationally accelerating jet (a self-destabilizing loop). For steady jet disintegration to occur by a similar self-destabilizing loop, the dispersive capillary wave produced by a surface energy release processes (jet tip contraction or Plateau–Rayleigh unstable wave growth) needs to take a form of steady capillary wave at a upstream location. Interestingly, figure 7 illustrates the formation of stationary wave elements with the horizontal yellow spot arrays shown near the nozzle exit. Quantitative characterization of this wave structure requires numerical simulations, which are described in the next section. The following explanation is based on the simulation results.

A TCCW formation duration is limited to a short interval, that begins the instant a new jet tip is produced by a short-wave breakup, and ends at the next short-wave breakup. Therefore, when we consider a single TCCW produced during the short interval, the TCCW falls in such a state that the jet tip which produced the TCCW is replaced by the newly produced jet tip before an element of the TCCW becomes a stationary one at a remote location. As a result, this TCCW interacts with the newly radiated TCCW and increase its amplitude as shown by the striped pattern after frame 6500, when short-wave breakups occur predominantly. This is a kind of parametric excitation like a swing or resonance. A stationary wave which has an upstream propagation speed equal to the local jet speed is eventually realizable in newly issued liquid, because a constant energy sustaining the stationary wave is continuously supplied from downstream by the successive short-wave breakups. The horizontal yellow spot arrays at certain intervals decreasing in the downstream direction show the stationary wave elements (with the nodal point at the nozzle exit) formed by a series of short-wave breakups. Since no TCCW sufficient to sustain a stationary wave structure is produced in the long-wave breakup phase, the stationary wave elements are convected downward and their wavelengths elongate to Plateau–Rayleigh unstable wave elements. This is why we can observe the parabolic-like red lines originating from the horizontal yellow spot arrays.

2.4.4. *Breakup sequence*

Figure 9(*a*) is a plot of the breakup wavelength against the breakup distance from the nozzle exit. For a few cycles of the jet length oscillation in figure 4, the breakup location x_B and wavelength λ_B of each breakup are measured from the high-speed images and plotted in figure 9(*a*). The breakup wavelength is defined as follows. For a long-wave breakup, which consists of two succeeding breakups forming a satellite drop, λ_B is the distance between the centres of the two bulging portions bridged by the breaking ligament and x_B is its mid-location. For a short-wave breakup which does not produce any satellite drop, λ_B is the length of the tip bulb and x_B is its centre location. This definition of short-wave breakup was strictly applied, regardless of whether a Plateau–Rayleigh unstable wave was superimposed on the jet or not.

In the figure, the wavelengths of the following three waves are expressed as functions of x for reference (see appendix A for their analytical expressions).

(i) Stationary wave with $(-v) = u$ (dashed line).

(ii) Neutral wave with $ka = 1$ (thick solid line). At a point x_N on this line, a TCCW element may become a Plateau–Rayleigh unstable wave element.

(iii) Unstable wave with maximum growth rate (dotted–dashed line).

https://doi.org/10.1017/jfm.2014.329 Published online by Cambridge University Press

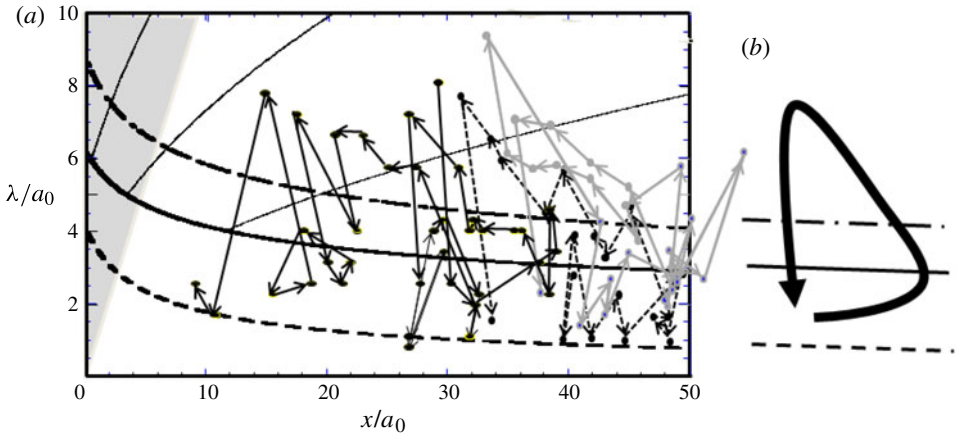


FIGURE 9. A series of breakups in the jetting-to-dripping transition viewed on a map classing the kind of wave, (*a*) shows the characteristic wavelengths excitable for the baseline jet. The thick dashed line denotes the wavelength of an upstream-propagating dispersive wave element which balances with the local jet velocity. The thick solid line denotes the wavelength of a dispersive wave element which turns to an unstable wave element. The thick dotted–dashed line denotes the wavelength of most unstable wave element. The thin broken lines denote the change in wavelength which each unstable wave element experiences, (*b*) represents the trend of jet disintegration change in a cycle of jet length oscillation.

A TCCW element which became an unstable wave at a point on the thick solid line increases its wavelength as it moves downstream. This wavelength change occurs along a thin solid line satisfying $ku = k_B u_B$.

The plots located between the dashed line and the thick solid line express short-wave breakups, while the plots above the thick solid line express long-wave breakups. Since the TCCWs produced by multiple short-wave breakups overlap and disturb some breakups, each series of breakup plots fluctuate irregularly. Nevertheless, it is apparent that a representative series of breakup plots in a cycle of smoothed jet length oscillation should take the form shown by the curved arrow in figure 9(*b*), indicating the short-wave breakup phase followed by the long-wave breakup phase. Figure 9(*a*) clearly indicates that the Plateau–Rayleigh unstable wave elements involved in the jetting-to-dripping transition are produced downstream of the nozzle exit. It is also found that the unstable wave element which causes the minimum jet length in a cycle of smoothed jet length oscillation has a breakup wavelength longer than that of the most unstable wave (above the dotted–dashed line).

2.4.5. *Initial amplitude of unstable wave element*

We assume that each long-wave breakup plotted in figure 9(*a*) occurs when the amplitude of the Plateau–Rayleigh unstable wave element grows up to the local radius a_B of the baseline jet at the breakup location x_B. Then, we can estimate its initial amplitude ε_N by applying the amplitude growth equation (see appendix A) along the thin solid line in figure 9(*a*). The calculation results are plotted with circles in figure 10. The two sets of circles express the unstable wave elements causing the series of long-wave breakups indicated in figure 9(*a*). Group A is for an early cycle while group B is for the cycle depicted in figure 6(*a*). The initial amplitude

https://doi.org/10.1017/jfm.2014.329 Published online by Cambridge University Press

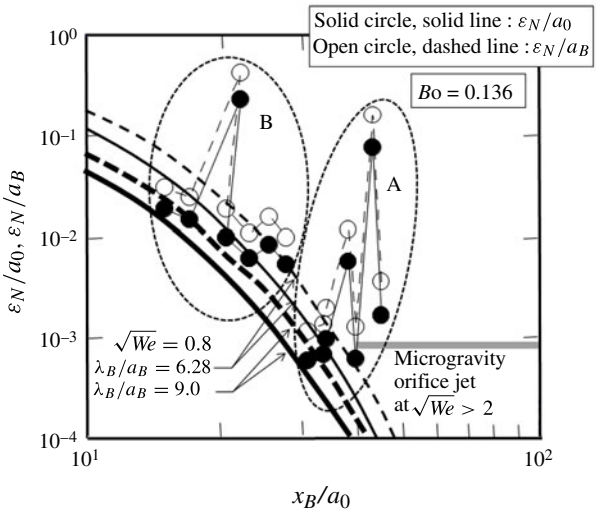


FIGURE 10. Initial amplitude ε_N of Plateau–Rayleigh unstable wave element disintegrating the jet at x_B. The circle plots are estimated from the breakup data for two cycles (A and B of smoothed jet length oscillation) in figure 9. The reference curves are for specified breakup wavelengths. Since the jet radius varies, two jet radii are used in their representation.

ε_N/a_0 increases from $O(0.001)$ to $O(0.01)$ as the jet length is shortened. Therefore, it is obvious that the jetting-to-dripping transition is caused by the increasing initial amplitude of the unstable waves with jet shortening.

For a given breakup wavelength λ_B/a_0, x_N/a_0 is determined as a function of x_B/a_0. In the figure, the dependences of ε_N/a_B on x_B/a_0 for the breakups of $\lambda_B/a_0 = 6.28$ and 9 are shown by the thin and thick black lines, respectively, for reference. The jet state at a large distance from the nozzle resembles the jet at a higher liquid issue speed. Therefore, the graphs indicate that the initial unstable wave amplitudes produced by the short-wave breakups at the higher liquid issue speed become very small. As a result, another self-destabilizing loop associated with the growth of the reproduced unstable wave with small initial amplitude (Umemura 2011) may operate dominantly and achieve jet disintegration at a fixed location on average. For example, the grey line shows the value for microgravity orifice jet experiments at $\sqrt{We} > 2$. In this case, the Plateau–Rayleigh unstable wave responsible for the constant breakup length must be produced at the orifice exit. Its initial amplitude is of the same order as that of the Plateau–Rayleigh unstable wave appearing at the start of the transition to dripping in the present laboratory experiment.

2.4.6. *Jetting-to-dripping transition mechanism*

Whenever a jet increases its length, a series of short-wave breakups may occur. This is true for all $\sqrt{We}$ values used in the present experiments. The jetting-to-dripping transition onsets under the condition that the short-wave breakups result in unstable wave elements that have larger initial amplitudes than those of the unstable waves responsible for the steady breakup distance. The self-destabilizing loop identified in figure 7 crucially relies on the presence of large jet acceleration; therefore, it may operate at a small value of $\sqrt{We}$. The oscillatory jet shortening observed in

https://doi.org/10.1017/jfm.2014.329 Published online by Cambridge University Press

the experiment is considered to be the only way by which the jet can be shortened from a long jet state, without the aid of external disturbances. A TCCW element destabilizing at a location close to the jet tip has a relatively large amplitude but does not have a travelling distance long enough to grow and shorten the jet significantly. A TCCW element moving downstream from a stationary wave location far from the jet tip is also unable to shorten the jet, because of its small amplitude and large elongation due to the accelerating jet flow. Only the TCCW elements destabilizing at intermediate distances are able to shorten the jet by long-wave breakups, which do not radiate any effective TCCWs. Therefore, there must be a period in which short-wave breakups occur and the jet is lengthened. As a result, the jet length oscillates when the jetting-to-dripping transition onsets from a long jet. As the TCCW-radiating jet tip approaches the nozzle exit, the initial amplitudes of the unstable waves produced from the TCCWs are increased accordingly, thus the jet shortening is accelerated. This self-destabilizing loop is completely deterministic.

3. One-dimensional model analyses

The striped pattern of figure 7 is totally different from what is predicted by conventional instability theories. To quantify the behaviours of TCCWs produced by a series of short-wave breakups, we performed one-dimensional model analyses and supported the physical interpretations described in the previous section.

3.1. *One-dimensional model equation*

It is assumed that the axial velocity $u(t, x)$ and pressure $p(t, x)$ are uniform at each cross-section x of the liquid jet. For an incompressible inviscid liquid, the equations governing the evolution of the local axial velocity $u(t, x)$ and jet radius $r(t, x)$ can be expressed as follows:

$$\rho\left[\frac{\partial u}{\partial t}+u\frac{\partial u}{\partial x}\right]=-\frac{\partial p}{\partial x}+\rho g,$$

$$p=\sigma\left[\frac{1}{r\sqrt{1+\left(\dfrac{\partial r}{\partial x}\right)^2}}-\frac{\dfrac{\partial^2 r}{\partial x^2}}{\left\{1+\left(\dfrac{\partial r}{\partial x}\right)^2\right\}\sqrt{1+\left(\dfrac{\partial r}{\partial x}\right)^2}}\right], \tag{3.1}$$

$$\frac{\partial r}{\partial t}+u\frac{\partial r}{\partial x}=-\frac{r}{2}\frac{\partial u}{\partial x}, \tag{3.2}$$

subject to

$$r\,(t, x=0)=a_0 \quad \text{and} \quad u(t, x=0)=U. \tag{3.3a,b}$$

Equation (3.1) is derived from Bernoulli's principle along the jet centreline, under the assumption that the jet centreline pressure is locally equal to the jet surface pressure. Therefore, the above equation system is appropriate to describe surface deformation with relatively large wavelength. Nevertheless, it is confirmed that the equation system can be used to satisfactorily describe TCCW radiation and short-wave breakup in comparison with a direct numerical simulation (Umemura 2011). Therefore, we apply it to an orifice jet, whose local axial velocity profile may be regarded as uniform to a good degree of approximation. Recently, the same type of one-dimensional equations including a viscous term are used by Rubio-Rubio, Sevilla & Gordillo (2013) for the linear global stability analysis of a viscous liquid jet at large Bond numbers to show a difference from the local linear stability analysis prediction.

https://doi.org/10.1017/jfm.2014.329 Published online by Cambridge University Press

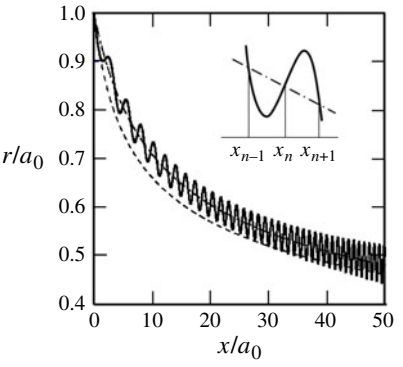


FIGURE 11. Steady solutions for $\sqrt{We} = 0.8$ and $Bo = 0.136$. The local jet radius r is expressed as a function of centreline coordinate x. The dashed line does not count any surface tension effect (free-fall dynamic solution). The axial velocity gradient at $x = 0$, obtained from this solution, is used to derive the other steady solutions with surface tension effect. The dotted–dashed line is the case when only the circumferential surface tension pressure is considered. The solid line counts both circumferential and axial surface tension effects. The inset explains how the nodal locations of this wavy surface deformation are defined.

3.2. *Steady jet flow solution*

Important information on stationary wave can be derived from a steady solution of (3.1)–(3.3).

Putting $\partial u/\partial t = \partial r/\partial t = 0$, (3.1) and (3.2) can be reduced to a second-order ordinary differential equation (ODE) for $r(x)$:

$$\frac{1}{2}\rho\left(\frac{Ua_0^2}{r^2}\right)^2 + p - \rho g x = \tfrac{1}{2}\rho U^2 + p\,(x=0)\,,$$
$$p = \sigma\left[\frac{1}{r\sqrt{1+(\mathrm{d}r/\mathrm{d}x)^2}} - \frac{\mathrm{d}^2 r/\mathrm{d}x^2}{\left\{1+(\mathrm{d}r/\mathrm{d}x)^2\right\}^{3/2}}\right]. \tag{3.4}$$

To integrate this from the injector exit $x = 0$, we have to specify the two unknown parameters $\mathrm{d}r/\mathrm{d}x(x=0)$ and $p(x=0)$. Various surface profiles are derivable depending on the combination of the two parameter values. An interesting solution for the case $\mathrm{d}r/\mathrm{d}x(x=0) = -Bo/2We = -0.106$ (estimated from (2.2)) and $\mathrm{d}^2r/\mathrm{d}x^2(x=0) = 0$ (i.e. $p(x=0)/(\sigma/a_0) = 1/\sqrt{1+(Bo/2We)^2} = 0.994$) is shown by the solid line in figure 11, which exhibits a wavy surface deformation whose wavelength decreases in the downstream direction. When p is represented by the circumferential surface tension pressure $p = \sigma/r$ in (3.4), we obtain an algebraic equation for r. This solution expresses a smooth surface profile $r = r_*(x)$ depicted by the dotted–dashed line and leads to $\mathrm{d}r_*/\mathrm{d}x(x=0) = -Bo/2/(We+1) = -0.0415$. It is noteworthy that the solid line oscillates about the dotted–dashed line. In the figure, (2.2) is also shown by the dashed line. Its behaviour is similar to the dotted–dashed line and validates the use of (2.2) in the previous section to estimate the local linear stability properties of the jet. The first-order differential equation, which is obtained by neglecting the axial surface tension effect, has no solution unless $\mathrm{d}r/\mathrm{d}x(x=0) < -Bo/2We$. Obviously,

https://doi.org/10.1017/jfm.2014.329 Published online by Cambridge University Press

this equation results in a physically unacceptable solution. We can also search for the combination of the two parameter values (e.g. $\mathrm{d}r/\mathrm{d}x(x=0) = -0.05\,750$, $p(x=0)/(\sigma/a_0) = 0.9871$, thereby, $a_0\mathrm{d}^2r/\mathrm{d}x^2(x=0) = 0.01\,135$) which results in a solution oscillating about the dotted–dashed line in the same fashion as the solid line, but with very small amplitudes (at most $0.002a_0$).

The wavy surface deformation must be produced by the capillary wave elements whose upstream propagation speed locally balances with the jet velocity. To check this, we calculated the half-wavelength of each stationary wave element from the neighbouring zeros of the deviation from the dotted–dashed line ($r - r_*$) as $\lambda_{1/2} = x_{n+1} - x_n$ ($n = 0, 1, 2, \ldots$). Then, we used (2.3) to estimate the upstream propagation speed ($-v$) of the half-wave element whose location is represented by the mid-location $x_{n+0.5} = (x_n + x_{n+1})/2$. That is, $v = \sqrt{\{\sigma/\rho r_*(x=x_{n+0.5})\}[\{\pi r_*(x=x_{n+0.5})/\lambda_{1/2}\}^2 - 1]}$. The ratio of ($-v$) to $u_*(x = x_{n+0.5})$ was unity within errors of 5 % for all wave elements. Thus, the following equation holds approximately:

$$\frac{\mathrm{d}x_{n+0.5}}{\mathrm{d}t} = -\sqrt{\frac{\sigma}{2\rho r_*\,(x=x_{n+0.5})}\left[\left\{\frac{\pi_* r_*\,(x=x_{n+0.5})}{x_{n+1}-x_n}\right\}^2 - 1\right]} + u_*\,(x=x_{n+0.5}) = 0. \quad (3.5)$$

It is remarkable that the finite-amplitude wavy surface deformation derived from the highly nonlinear equation satisfies the dispersion relation (2.3) derived from the local linear stability analysis. This implies that the stationary wave amplitude is determined corresponding to the amount of energy transferred from downstream by the upstream-propagating capillary wave.

An important implication of the wavy steady solutions is that upstream-propagating capillary waves, continuously produced around a downstream location, tend to form a train of stationary wave elements, as illustrated in figure 11. The horizontal yellow spot arrays observed in figure 7 are considered to be produced in this way. In fact, the arrowed red horizontal lines drawn on the left-hand side of figure 7, show the necked locations of the solid line in figure 11, which are consistent with the horizontal yellow spot array locations. These stationary wave elements are convected downstream when they lose the energy supply from downstream.

3.3. *Jetting-to-dripping transition simulation of orifice jet*

The targeted region of linear stability analysis is a continuous liquid column with small surface deformation and excludes the important energy source portion, i.e. the jet tip, where nonlinearity is dominant. Therefore, the downstream boundary of the linear region must vary with time, but it is difficult to *a priori* know the boundary location and the condition to be imposed there. This is why the wave properties deduced from local linear stability analysis were used to consider the TCCW behaviours in the previous section. Our experimental results clearly indicate that the downstream boundary of the linear region is not described by the so-called free boundary condition. Instead, the jet tip may be the energy source that causes the unstable phenomena occurring in the linear region. In order to demonstrate this possibility and to examine the TCCW behaviours in the jetting-to-dripping transition process of an orifice jet in detail, we solved equation system (3.1)–(3.3) numerically by incorporating algorithms mimicking the round jet tip and jet disintegration. The calculation method and some calculation results for numerical validation are presented

https://doi.org/10.1017/jfm.2014.329 Published online by Cambridge University Press

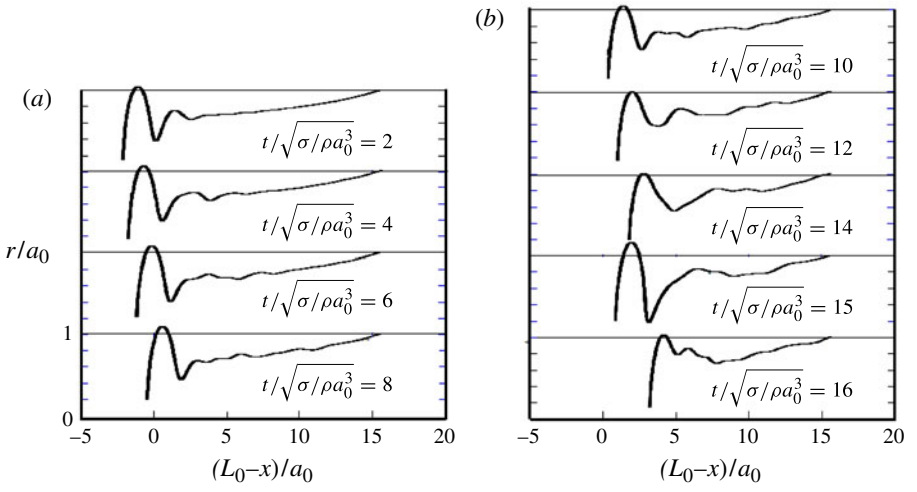


FIGURE 12. Temporal evolution of liquid jet shape in the initial value problem simulation for the case of $\sqrt{We} = 0.8$, $Bo = 0.136$ and $L_0/a_0 = 19$. As explained in appendix B, a minor-spherical surface region is attached to the one-dimensional model liquid column in order to express the jet tip. Its size can be identified with the gap to the centreline. Several short-wave breakups occur in the figure.

in appendix B. Here we explain the result of an initial value problem calculation and characterize the TCCWs produced by a series of short-wave breakups.

The present calculation cannot simulate the nozzle jet jetting-to-dripping transition feature in general. However, the essential feature of figure 7 (just before transition to dripping) can be captured with this calculation. We calculated the case of liquid issue speed $\sqrt{We} = 0.8$ and initial jet length $L_0/a_0 = 19$, which corresponds to the condition that the steady breakup length of orifice jet in figure 1(*b*) is extrapolated to $\sqrt{We} = 0.8$. In this condition, the value of $\sqrt{\rho u^2 r_*/\sigma}$ at the jet tip location becomes smaller than 1.7. It is expected from figure 1(*a*) that both orifice and nozzle jets exhibit similar breakup behaviours (mainly short-wave breakups). Thus, the initial value problem of this case describes the TCCW structure, formed by a newly started series of short-wave breakups in figure 6(*b*) and after frame 6900 in figure 7, provided that the unstable waves and TCCWs produced earlier are all eliminated.

Figure 12 shows the evolution of the surface deformation along the jet calculated for the initial value problem, in which the smooth orifice jet expressed by the steady solution $[r_*(x), u_*(x)]$ (the dotted–dashed line in figure 11) was taken as a hypothetical initial undisturbed jet state. The jet tip location history of the subsequent jetting-to-dripping transition process can be seen in figure 15. The calculated jet surface deformation caused by the jet tip contraction is generally consistent with that observed on the high-speed camera images at $\sqrt{We} = 0.9$. Here, we note the presence of some small-amplitude deformation near the injector exit. The figure is largely stretched in the vertical direction. However, the surface deformation is still not noticeable. The surface near the injector exit looks smooth on the scale of the whole jet. However, as mentioned before, if we estimate the initial amplitude of the Plateau–Rayleigh unstable wave at the injector exit in the microgravity orifice jet experiment with $\sqrt{We} = 2$ (figure 1), the average breakup length $L_B/a_0 = 40$ leads to $\varepsilon_0/a_0 = 8.5 \times 10^{-4}$. This implies that such a small surface deformation may yet

https://doi.org/10.1017/jfm.2014.329 Published online by Cambridge University Press

play an important role in jet disintegration. Therefore, it is necessary to examine the upstream surface deformation with fine resolution. In the following we examine the surface deformation evolution in more detail and validate the physical ideas used to interpret the experimental results in the previous section.

Figure 13 shows the temporal evolution of the surface deformation magnitude $|r(t, x) - r_*(x)|/a_0$ until $t\sqrt{\sigma/\rho a_0^3} = 10$, during which five short-wave breakups occur. Based on this figure, the TCCW behaviours characteristic to the gravitationally accelerating jet can be quantitatively examined by discarding contributions intrinsic to the initial jet set-up. Figure 13(i)–(iii) show the results before the first breakup at $t\sqrt{\sigma/\rho a_0^3} = 2.5$. Figure 13(iv) shows three instants after the first breakup. The nodal locations of the steady wavy surface deformation (figure 11) are indicated by the vertical dashed lines for reference. In the upper right of the graphs, arrowed horizontal lines show the frontal location of the newly issued liquid at the instants t for the respective plots. Each frontal location was determined based on the free-fall equation $x = Ut + 0.5gt^2$.

The following is found from each panel of figure 13.

In figure 13(*a*), the initial jet tip is a mathematical singular point and produces dispersive capillary wave elements with very small amplitudes and wavelengths. In principle, such short waves cannot be described accurately by the present one-dimensional model. Nevertheless, figure 13(*a*) indicates that the present calculation results in a mathematically correct solution of equation system (3.1)–(3.3) with sufficient resolution. The short wave elements have a very large upstream-propagating speed determined from the dispersion relation $\omega = k^2$. Therefore, the initial TCCW is unaffected by the jet flow and described by the solution

$$\hat{\delta}\left(\hat{t}, \hat{x}\right) = \int_0^{\hat{t}} f(\hat{t} - \hat{\tau}; \hat{\xi} \to 0) \frac{\cos\left(\dfrac{\hat{x}^2}{4\hat{\tau}}\right)}{\sqrt{\hat{\tau}}} \mathrm{d}\hat{\tau} \tag{3.6}$$

as seen in region B, which initially occupies the whole jet region, excluding the ends. The function f corresponds to an energy flux caused by the jet tip contraction. Only the late evolution of the TCCW observed in region A, which extends toward the injector as time passes, is of concern in the present study.

In region C, there is a relatively long wave, on which the continued short wave of (3.6) and its reflection at the injector exit are superimposed. This long wave is produced by the fact that the initial jet flow (figure 11) is not an exact steady solution of equation system (3.1)–(3.3). Therefore, it grows in the region where the initial liquid exists, and its influence penetrates into the newly issued liquid satisfying the boundary condition at the injector exit. Since this initial jet-modifying wave develops from the upstream to downstream direction, its wavelength increases with time. Obviously, the initial evolution of this wave should be independent of the initial jet length.

In figure 13(*b*), we see that as time passes, the dispersive capillary wave increases its wavelength and decreases its upstream propagation speed. Therefore, the evolution of the TCCW in region A comes to be significantly influenced by the jet flow structure. The figure indicates that the amplitude of the TCCW elements in region A decrease exponentially with increasing distance from the jet tip, accompanied by a gradual variation due to the Rayleigh oscillation of the jet tip liquid bulb. The momentarily stationary wave element, which is identifiable in reference to the vertical

https://doi.org/10.1017/jfm.2014.329 Published online by Cambridge University Press

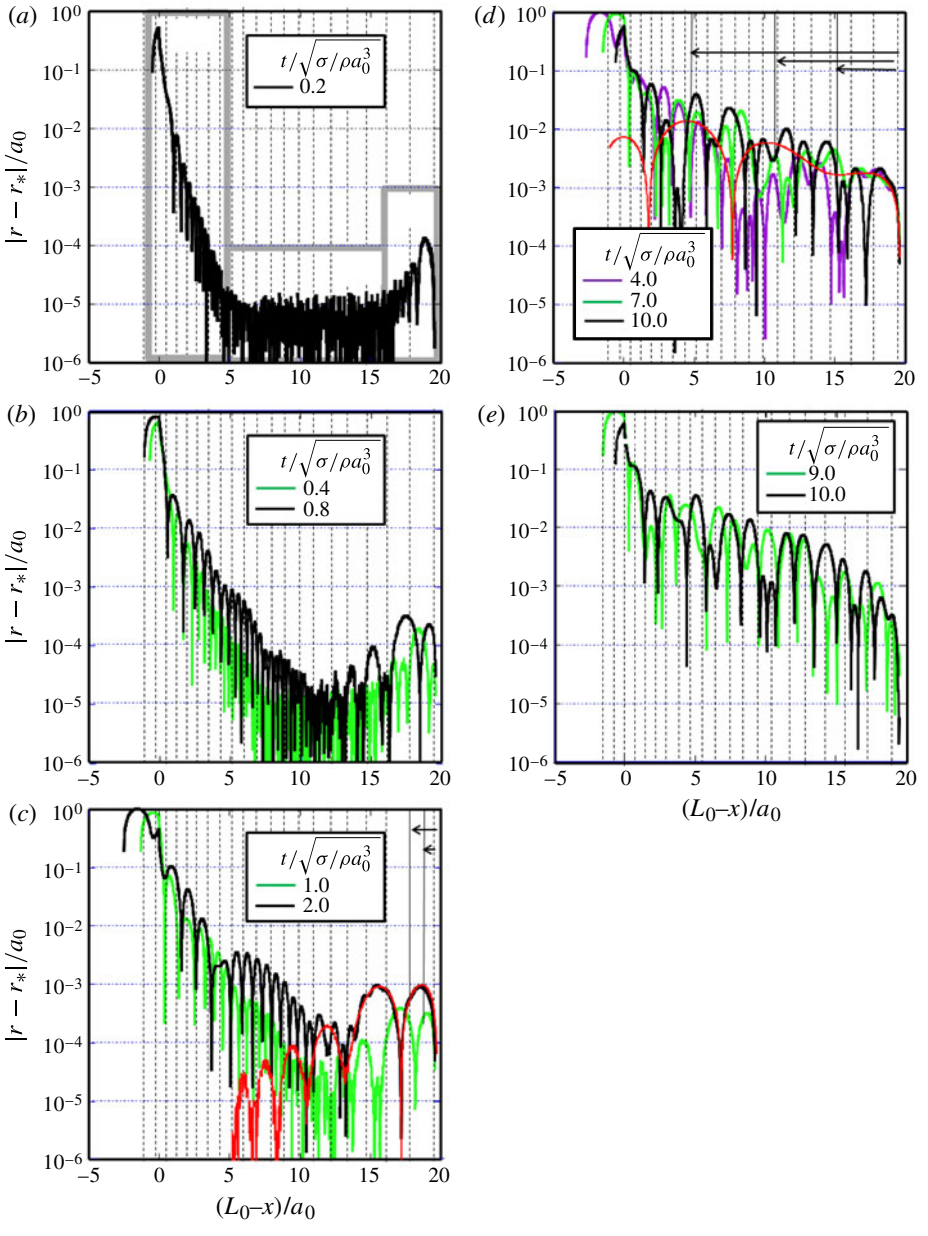


FIGURE 13. Temporal evolution of surface deformation magnitude in the initial value problem simulation for the case of $\sqrt{We} = 0.8$ and $L_0/a_0 = 19$. (*a*)–(*d*) The state before the jet liquid is completely replaced by the newly issued liquid. The arrows show the penetration length of newly issued liquid. The vertical dotted lines express the nodal locations of the stationary waves expressed by the solid line in figure 11. The red line shows the surface deformation developing from the injector exit due to the use of the initial jet state which is not an exact solution of the governing equations. (*e*) The surface deformation magnitude in the case when this surface deformation is subtracted to show the pure TCCW behaviours.

https://doi.org/10.1017/jfm.2014.329 Published online by Cambridge University Press

dashed lines, is first established near the jet tip and then at a more upstream location. Consistent with figures 6 and 7, the stationary wave element produced near the jet tip is elongated and tends to become steady relative to the jet tip, which moves in the downstream direction.

In figure 13(*c*) the black line expresses the surface deformation near the first short-wave breakup at $t\sqrt{\sigma/\rho a_0^3} = 2.5$. To distinguish the initial jet-modifying wave, we conducted the same calculation for $L_1/a_0 = 81$, the result of which is indicted by the red line. At $t\sqrt{\sigma/\rho a_0^3} = 2$, no significant TCCW of this case reaches the illustrated region. It is found that the red line coincides with the black line near the injector exit (in region C). The difference of the black line from the red line at $(L_0 - x)/a_0 < 13$ expresses the developed TCCW of the $L_1/a_0 = 19$ case.

Figure 13(*d*) shows the wave structure after several short-wave breakups. By a short-wave breakup, another TCCW is radiated from the newly produced jet tip and superimposed on the previous TCCW which has lost its own jet tip (energy source). The new TCCW excites the old TCCW by a similar mechanism to a swing. As a result, it appears that the old TCCW continues to develop and transfer energy in the upstream direction. At $t\sqrt{\sigma/\rho a_0^3} = 10$, when a considerable portion of the jet has been replaced by the newly issued liquid, the initial jet-modifying wave spans more than half the jet length as indicated by the red line, while the black surface deformation line exhibits several peaks within it. This implies that the TCCW elements with larger amplitudes have developed over the whole jet region.

In figure 13(*e*), to extract the TCCW state around $t\sqrt{\sigma/\rho a_0^3} = 10$, we subtracted the initial jet-modifying wave from the surface deformation $r - r_*$. Its absolute value is depicted in figure 13(*e*). It is found that a stationary wave is formed around $x/a_0 = 7$. This means that the TCCWs produced by a series of short-wave breakups behave like a single TCCW which transfer an amount of the surface energy released by the jet tip contraction and deforms the surface of newly issued liquid. Downstream of the stationary wave element, the wave elements having a longer wavelength than the local stationary wavelength move in the downstream direction. Such a TCCW structure is observed after the initial jet liquid is replaced by newly issued liquid and endorses the formation of stationary wave elements over a jet region apart from the jet tip in the short-wave breakup phase shown in figure 7. It is notable that the amplitudes of TCCW elements in figure 13(*e*) are in the same range of initial unstable wave amplitude estimated in figure 10. They take a exponentially smaller value nearer to the injector exit.

The wavelengths of TCCW elements in figures 7 and 13 can be compared by referring to the steady-solution wavelength distribution included in the two figures. Good consistency is observed to conclude the following physics underlying figure 7.

(i) Since the stationary waves must be produced in the newly issued liquid, their formation and maintenance near the injector exit require a constant energy supply from downstream. This energy is supplied by the TCCW radiations due to a series of short-wave breakups around a fixed location in a cycle of smoothed jet length oscillation.

(ii) The TCCW elements near the jet tip become steady relative to the jet tip and enhance the occurrence of short-wave breakup.

(iii) In between these two kinds of steady TCCW elements, there exist TCCW elements which, after reaching a momentarily stationary wave location, are elongated to Plateau–Rayleigh unstable waves in the course of their downstream

https://doi.org/10.1017/jfm.2014.329 Published online by Cambridge University Press

movement. Since the unstable wave elements moves at the local jet velocity, they may pass the steady capillary wave elements with upstream propagation speed.

The long breakup wavelengths observed about $t\sqrt{\sigma/\rho a_0^3} = 20$ in figure 15(*b*) are caused by the presence of such Plateau–Rayleigh unstable wave elements. Interestingly, this elapsed time $t\sqrt{\sigma/\rho a_0^3} = 20$ roughly corresponds to the short-wave breakup phase period of the smoothed jet length oscillation observed in the experiment.

3.4. *Difference from orifice jet case*

Figures 6 and 7 are for the nozzle jet. The most important difference from the orifice jet is the presence of a velocity profile in the issued liquid jet. Finally, we discuss the modification caused by this difference, which should be taken into consideration in the physical interpretation of figure 7.

The time τ, necessary for the velocity profile of each liquid jet element to relax to a uniform velocity, is estimated from the condition $K\sqrt{\nu\tau} = 0.719a$, where ν is the dynamic viscosity. During this period, the jet element travels a distance $(U\tau + 0.5g\tau^2)/a_0 = \sqrt{We}/(K^2Oh) + Bo/(2K^4Oh^2) = 214/K^2 + 4890/K^4$. If we use the value of K which is adopted in the entrance length formula (Sparrow, Lin & Lindgren 1964; Fargie & Martin 1971), i.e. $1/(4K^2) = 0.065$, the dimensionless relaxation distance becomes 96.54, which is much longer than the maximum jet length in the present experiment. Therefore, there is a possibility that the wave structure is influenced by the velocity profile. It is known that the instability property is almost the same as that of a plug-flow profile jet if the difference between the surface velocity u_s and the centreline velocity u_m satisfies $\rho(u_m - u_s)^2 a/\sigma < 1$ (Umemura *et al.* 2011), which is the case everywhere in the present experiment. Thus, the velocity profile only slightly reduces the growth rate of Plateau–Rayleigh unstable wave. However, it should be noted that the early TCCW behaviour must be modified significantly from the orifice jet case for the reasons described in the next two paragraphs. The wetting of the nozzle end does not influence the global jet instability, since the range of influence of the meniscus is at most in the order of the nozzle tube thickness.

The microgravity jet experiments (figure 1) suggest that, when the jet tip is located at a location where the value of $\sqrt{\rho u^2 a/\sigma}$ becomes smaller than 1.6, the jet length is not increased by short-wave breakup. Instead, the repeated short-wave breakups may shorten the jet length and the jet transitions to dripping under normal gravity. This is the jetting-to-dripping transition mechanism proposed by Clanet & Lasheras (1999). For the orifice jet, the extrapolated steady breakup length satisfies this condition at $\sqrt{We} = 0.9$ and the proposed mechanism is applicable, as confirmed in our laboratory experiments and in the calculations detailed in appendix B. However, for the nozzle jet, the value of $\sqrt{\rho u^2 a/\sigma}$ estimated at the jet tip location of transition onset is considerably greater than 1.6. Therefore, the early shortening of the jet length must be due to Plateau–Rayleigh unstable waves as observed in figures 6 and 7. The presence of the velocity profile affects the jet flow instability by changing the early TCCW behaviour from that of the orifice jet in the following way.

For an undisturbed jet, the energy source is the jet tip contraction only. When we consider the TCCW in the nozzle jet, the behaviour of the short-wave elements is not correctly described by equation system (3.1)–(3.3). The surface deformation of wavenumber k is only associated with the liquid layer of thickness $O(1/k)$ from the surface. Therefore, for the nozzle jet in a velocity profile relaxation process, short TCCW elements with $kr > 1$ are affected by the jet surface velocity, which is smaller

https://doi.org/10.1017/jfm.2014.329 Published online by Cambridge University Press

than the central velocity. This means that the degree of liquid acceleration felt by the early TCCW is greater than that in the orifice jet and the TCCW can propagate further upstream. As a result, a TCCW structure similar to that in an orifice jet is realizable for a longer nozzle jet. This is why the transition can onset at a longer jet length. The formation of Plateau–Rayleigh unstable waves takes place where these TCCWs are elongated significantly. The consistence of the stationary wave observed in figure 7 with the steady wavy surface deformation in figure 11 indicates that the finally established, relatively long-wave structure can be successfully described by the one-dimensional model regarding the average axial velocity as the assumed uniform axial velocity.

The growth of a Plateau–Rayleigh unstable wave can play a similar role to the jet tip contraction as an energy supplier. The experimentally observed steady wave structure formed by TCCWs, thus, also supports the steady realization of a similar, but very small-amplitude wave structure in the newly issued liquid by the continuously and periodically dispersive capillary wave radiation from the reproduced, growing unstable wave. This is a self-destabilizing loop realizing the steady breakup length of low-speed nozzle and orifice jets proposed by Umemura (2011) and Umemura *et al.* (2011). The present experiments clearly show that the highly disturbed downstream state disturbs the upstream state (following causality) and produces convectively unstable waves (gaining energy from the surface) resulting in the downstream disturbed state.

4. Conclusion

The jetting-to-dripping transition of a nozzle jet was utilized to experimentally visualize the behaviours of dispersive capillary waves produced by jet tip contraction. The jet tip contraction is a nonlinear process that cannot be described, in linear stability analysis, as other than the energy source to the upstream-propagating dispersive wave. It was found that a cyclic of the smoothed jet length oscillation observed in the experiment represents a self-destabilizing loop operating in the gravitationally accelerating jet. The cycle consists of two phases. In the first phase when the jet is disintegrated by a series of short-wave breakups, the jet length increases because the local baseline jet speed at the instantaneous jet tip location is larger than the recession speed of the jet tip which is newly produced upon every short-wave breakup. Part of the surface energy released by the jet tip contraction is transferred upstream through the TCCW radiated from the jet tip. Each TCCW element is elongated by the gravitationally accelerating jet flow and may change to a Plateau–Rayleigh unstable wave element. Therefore, in the next phase the jet disintegrations caused by the amplified Plateau–Rayleigh unstable wave elements shorten the jet length. The Plateau–Rayleigh unstable wave elements produced nearer the nozzle exit have smaller amplitude than those produced downstream even near the jet tip. Hence, the short-wave breakup phase is recovered. The numerical simulations based on the one-dimensional mode could reveal that a later radiated short TCCW excites the existing elongated TCCW like a swing. As a result, the TCCWs radiated by a series of short-wave breakups may produce the stationary wave elements far from the jet tip, which move downstream and become Plateau–Rayleigh unstable wave elements as the energy supply from the jet tip ceases. In principle, the self-destabilizing loop revealed in the present study is completely deterministic because the initial amplitude of each Plateau–Rayleigh unstable wave element is determined by the energy transferred from the contracting jet tip. Therefore, the nozzle

https://doi.org/10.1017/jfm.2014.329 Published online by Cambridge University Press

flow noises which are believed to be the origin of Plateau–Rayleigh unstable wave in the conventional stability analysis have nothing to do with the jet disintegrations in the experiment.

In general, advances in fluid dynamic instability theory crucially rely on the methods of treating dispersive waves. Low-speed water jets enable us to observe excited dispersive waves manifested as surface deformations. This study was an effort to better understand low-speed water jets. The experimental results demonstrated that a downstream nonlinear process may be the energy source to produce a convectively unstable wave in an upstream region to which linear stability analysis is applicable.

Acknowledgements

The present study was supported by a Grant-in Aid for Scientific Research from the Ministry of Education, Culture, Sports, Science and Technology of Japan and by the 'Ground-based Research Program for Space Utilization' promoted by the Japan Space Forum.

Appendix A. Unstable wave characteristics based on local stability analysis

Since an unstable wave element moves at the local jet velocity, its wavelength $\lambda = 2\pi/k$ is elongated according to

$$ku = k_B u_B. \tag{A 1}$$

Equations (2.2), (2.3) and (A 1) enable us to express the local unstable wave characteristics as functions of the instantaneous unstable wave location x as shown below.

A TCCW element changes to an unstable wave element at the location x_N satisfying $k_N a_N = 1$. Thus,

$$\frac{\lambda_N}{a_0} = 2\pi\frac{a_N}{a_0} = 2\pi\left(1 + \frac{2Bo}{We}\frac{x_N}{a_0}\right)^{-1/4}. \tag{A 2}$$

From (2.3), the growth rate γ of each unstable wave element is expressed as $\gamma = k\sqrt{(\sigma/2\rho a)\{1-(ka)^2\}}$. The growth rate maximizes where the wavelength satisfies the condition $k_M a_M = 1/\sqrt{2}$, yielding

$$\frac{\lambda_M}{a_0} = 2\sqrt{2}\pi\frac{a_M}{a_0} = 2\sqrt{2}\pi\left(1 + \frac{2Bo}{We}\frac{x_M}{a_0}\right)^{-1/4}. \tag{A 3}$$

An unstable wave element lengthens its wavelength according to

$$\frac{\lambda}{a_0} = \frac{u}{u_B}\frac{\lambda_B}{a_0} = \frac{u}{u_B}2\pi\frac{a_N}{a_0}\frac{u_B}{u_N} = 2\pi\sqrt{1 + \frac{2Bo}{We}\frac{x}{a_0}}\left(1 + \frac{2Bo}{We}\frac{x}{a_0}\right)^{-3/4} \tag{A 4}$$

where subscript B refers to breakup location. The surface deformation amplitude of each unstable wave element obeys

$$\varepsilon = \varepsilon_N \exp\left(\int_{x_N}^{x}\frac{\gamma\,\mathrm{d}x}{u}\right) = \varepsilon_N \exp\left(\frac{St}{\sqrt{2We}}\int_{x_N/a_0}^{x/a_0}\left(\frac{U}{u}\right)^{7/4}\sqrt{1 - St^2\left(\frac{U}{u}\right)^3}\,\mathrm{d}\hat{x}\right) \tag{A 5}$$

https://doi.org/10.1017/jfm.2014.329 Published online by Cambridge University Press

where $St = k_B u_B a_0/U$. Evaluating (A 5) at a breakup location x_B where ε becomes equal to the local jet radius a_B, we obtain

$$\frac{\varepsilon_N}{a_B} = \exp\left[-\frac{St}{\sqrt{2We}}\int_{x_N/a_0}^{x_B/a_0}\left(\frac{U}{u}\right)^{7/4}\sqrt{1-St^2\left(\frac{U}{u}\right)^3}\,\mathrm{d}\hat{x}\right]$$
$$= \exp\left[-\frac{St\sqrt{We}}{\sqrt{2}Bo}\int_{St^{2/3}}^{(\lambda_B/2\pi a_0)St}\left(\frac{U}{u}\right)^{3/4}\sqrt{1-St^2\left(\frac{U}{u}\right)^3}\,\mathrm{d}\left(\frac{u}{U}\right)\right]. \quad \text{(A 6)}$$

Appendix B. One-dimensional numerical calculation of a disintegrating orifice jet

B.1. *Calculation method*

Equations (3.1) and (3.2) were solved using a staggered grid system, on which the partial differential equations were spatially discretized. The grid size Δx was selected to be $(1/40)_a$, based on a practical calculation performance to resolution tradeoff. The time step used in the temporal Runge–Kutta integration was $\Delta t = 0.01\Delta x^3\sqrt{\rho/\sigma a_0^3}$.

As shown in figure 14, the round jet tip was expressed as a minor spherical surface region, in which the axial velocity and pressure are uniform. The grid point x_{ntip}, where the minor spherical surface region is connected to the upstream jet region governed by the discretized (3.1) and (3.2), was changed when the jet tip P moved beyond the neighbouring grid point x_{ntip+1} or x_{ntip-1}. The axial velocity of the minor spherical surface region was equated to that defined at $x = (x_{ntip-1} + x_{ntip})/2$. The curvature radius R_0 of the minor spherical surface, which specifies the jet tip pressure $(2\sigma/R_0)$, was determined in such a way that the jet tip surface smoothly connects with the upstream jet surface. To avoid possible high-frequency oscillation due to the capillary wave transmission between the attached tip region and the upstream jet region, the curvature radius R_0 at each time step was determined by averaging over the previous three time step values.

In the present problem, the jet disintegration is indispensable. It is especially important that the contraction process of the jet tip which is newly produced by a short-wave breakup is described appropriately. Therefore, we devised a means of achieving this. In the two-phase flow calculation using the surface tension force replaced by a body force, liquid jet disintegration is automatically achieved by the overlapping of the two body force regions. In the present one-dimensional model, we have to incorporate an algorithm which mimics the disintegration. We can search the most necked portion at each time step and find the minimum radius of the most necked portion, r_{min}, and its axial location, x_{min}. When r_{min} became smaller than a fraction ϕ of the local jet radius $r_*(x = x_{min})$ of the steady solution (the dotted–dashed line in figure 11), the jet was cut there as illustrated in figure 14. This computational jet disintegration was done at the next time step by creating a new minor spherical surface that is tangent to the upstream liquid column at the inflection point I of the most necked surface portion. This new surface is expressed by the dashed line in the figure. The axial velocity in the jet region defined by the dashed line was uniformly equated to the value of axial velocity at the axial location of point I. Since the values of surface radius and axial velocity are given at each grid points in the region, the jet tip treatment algorithm can be used to calculate the subsequent jet tip behaviour. Using a small value of ϕ, this algorithm enables us to simulate a long-wave breakup (two-staged breakups generating a satellite drop) as well. However, this calculation

https://doi.org/10.1017/jfm.2014.329 Published online by Cambridge University Press

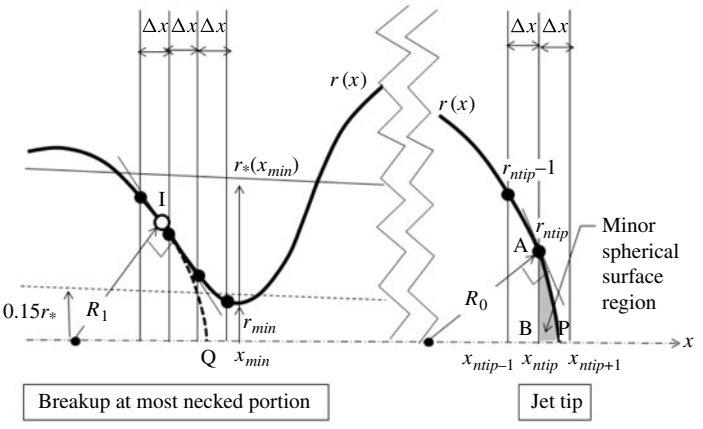


FIGURE 14. Jet tip and jet disintegration treatments. The minor spherical surface region PAB attached to the one-dimensional model liquid column serves as the role of contracting jet tip. Point I denotes the upstream inflection point of the surface profile at the most necked portion. Once the newly produced tip surface (dashed line IQ) is determined by the normal R_1 to the surface at point I, the jet tip algorithm can be used to calculate the subsequent jet tip behaviour. The discretized axial velocity is defined at the mid-point between neighbouring grid points at which the discretized surface radius is defined.

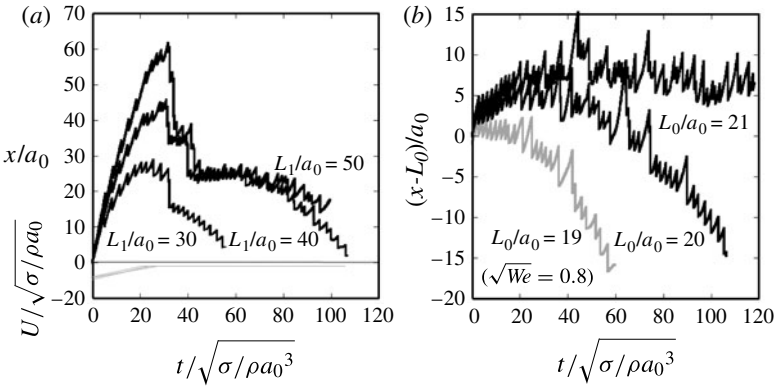


FIGURE 15. Jet tip location histories in the case of $\sqrt{We} = 0.9$ and $Bo = 0.136$. (*a*) Simulations mimicking the laboratory orifice jet experiment by changing the liquid issue speed as shown by the grey line. The parameter L_1 specifies the initial liquid issue speed. (*b*) Initial value problem simulation. The liquid jet of length L_0 is initially in the steady flow state corresponding to the dotted–dashed line in figure 11. As the newly issued liquid occupies the whole jet region, the jet settles down to a state independent of the initial state.

needs a much finer grid system. Therefore, in the present study in which we are interested in the behaviours of TCCWs radiated by a series of short-wave breakups, we set $\phi = 0.15$ and forced all jet breakups to occur as a breakup radiating a TCCW. As a result, the smoothed jet length oscillation does not emerge in the present simulation. There is another more important reason for setting $\phi = 0.15$. This

https://doi.org/10.1017/jfm.2014.329 Published online by Cambridge University Press

is associated with the description of short-wave breakups in the one-dimensional model. The short-wave breakup mechanism is detailed in Umemura (2011). When the necked portion connected to the tip liquid bulb is locally destabilized according to Bernoulli's principle, a high-speed liquid jet flowing into the tip liquid bulb pinches the neck further. Then, because of the jetting liquid inertia, the downstream necked portion cuts into the round upstream surface of the tip liquid bulb and the surface radius of the tip liquid bulb at that portion becomes two-valued. In general, the one-dimensional model equation tends to simulate this process precisely, so that the calculation breaks down just before the two-valued surface radius appears. The selection of $\phi = 0.15$ avoids this calculation breakdown. As a result, the short-wave breakup period is underestimated (by at most 30 %) compared with the experimental value. The calculation contains no adjusting parameters other than ϕ.

B.2. *Calculation results*

We considered orifice jets with the conditions of $\sqrt{We} = 0.9$ and $Bo = 0.136$ (figure 15). This is the case when the orifice jet transitions from jetting to dripping (see figure 3). Therefore, it is obvious that the start of liquid issue from the orifice at this condition does not form a jet. We confirmed this in the calculation.

We conducted the following two kinds of calculation.

(*a*) Liquid issue mimicking our single issue speed experiment.

In our experimental apparatus, piston movement at a specified speed initially pressurizes the injector liquid, so that the initial liquid, issue speed takes a considerably large value to form a jetting liquid, which is subsequently stretched as the liquid issue speed reduces to the specified value. In an idealized fashion, this transient process is mimicked as follows. Initially, g in the momentum equation is equated to zero and the instantaneous liquid issue speed U is changed with time according to $U = U_0 - gt$. When U becomes equal to the specified value $U_1 = \sqrt{We\sigma/(\rho a_0)}$ at time $t = T$, the calculation is continued by changing g from zero to the gravitational acceleration value and fixing the liquid issue speed at U_1. The deceleration period T is determined by $T = \sqrt{2(L_1 - L_0)/g}$, where L_1 is a target jet length which may be arbitrarily set and $L_0 = a_0$. Therefore, the initial liquid issue speed is $U_0 = U_1 + \sqrt{2(L_1 - L_0)g}$.

The calculation results for $L_1/a_0 = 50$, 40 and 30 are shown in figure 15(*a*). Similar to the jet tip location history obtained in our experiment, the jet is initially lengthened repeating short-wave breakups. Then, the Plateau–Rayleigh instability caused by the jet stretching disintegrates and shortens the jet to a certain length around $25a_0$. This temporally fixed breakup length is consistent with the value at $\sqrt{We} = 0.9$ extrapolated from the experimentally measured steady breakup length. After that, the jet length is shortened at an accelerated rate. This behaviour is similar to the jetting-to-dripping transition observed in figure 3. When L_1/a_0 is increased, the degree of initial jet length overshoot becomes greater but the later transition behaviour is similar. When L_1/a_0 is decreased, the less overshot jet length drops to a value at a late stage of the jetting-to-dripping transition of a larger L_1/a_0 case. The agreement with the experimental observation is remarkable, which demonstrates that the self-destabilizing mechanism may consist of the fluid dynamic processes governed by equation system (3.1)–(3.3).

(*b*) Initial value problem.

The jet length is always finite. We examined what happens subsequently if a finite length of jet at an instant ($t = 0$) were in a hypothetical undisturbed steady state. As the initial jet state, the steady solution $[r_*(x), u_*(x)]$ (the dotted–dashed line in

https://doi.org/10.1017/jfm.2014.329 Published online by Cambridge University Press

figure 11) was adopted for the initial jet lengths of $L_0/a_0 = 21$ and 20. The case of $\sqrt{We} = 0.8$ and $L_0/a_0 = 19$ was also calculated and the text treats this case. The calculation results are shown in figure 15(*b*). We first note the overall trend. Until $t\sqrt{\sigma/\rho a_0^3} = 15$, all of the initial liquid goes out of the calculation region due to jet disintegration. When the newly issued liquid occupies the whole jet region, the jet flow eventually becomes independent of the initial jet state. In the case of $L_0/a_0 = 21$, the jet length gradually increases up to the same value as the temporally settled jet length in figure 15(*a*). In the case of $L_0/a_0 = 20$, the jet transitions to dripping earlier. It is found that, once short-wave breakup has occurred enough times, the same length of jet exhibits the same jet disintegration behaviour in both figure 15(*a*,*b*). This demonstrates that the jet tip contraction, which necessarily appears in the jet formation process, plays an important role in forming the eventual wave structure that results in a steady breakup length or a transition to dripping. No external excitations such as nozzle flow disturbances are necessary to realize this jet state.

REFERENCES

AMAGAI, K. 2000 Instability theory of circular liquid jet. *Atomization* **9**, 261–269 (in Japanese).

ANNA, S. L., BONTOUX, N. & STONE, H. A. 2003 Formation of dispersions using flow focusing in microchannels. *Appl. Phys. Lett.* **82**, 364–366.

ASHGRIZ, N. & MASHAYEK, F. 1995 Temporal analysis of capillary jet breakup. *J. Fluid Mech.* **291**, 163–190.

BACHELOR, G. K. 1958 *Collected Works of G.I. Taylor*. Cambridge University Press.

BLASISOT, J. B. & ADELINE, S. 2003 Instabilities on a free falling jet under an internal flow breakup mode regime. *Intl J. Multiphase Flow* **29**, 629–653.

CHANDRASEKHAR, S. 1961 *Hydrodynamic and Hydromagnetic Stability*. Clarendon.

CLANET, C. & LASHERAS, J. C. 1999 Transition from dripping to jetting. *J. Fluid Mech.* **383**, 307–326.

COULLET, P., MAHADEVAN, L. & RIERA, C. S. 2005 Hydrodynamical models for the chaotic dripping faucet. *J. Fluid Mech.* **526**, 1–17.

DEBLER, W. & YU, D. 1988 The breakup of laminar liquid jets. *Proc. R. Soc. Lond.* A **415**, 107–110.

EGGERS, J. 1997 Nonlinear dynamics and breakup of free surface flows. *Rev. Mod. Phys.* **69**, 865–930.

EGGERS, J. & DUPONT, T. F. 1994 Drop formation in a one-dimensional approximation of the Navier–Stokes equation. *J. Fluid Mech.* **262**, 205–221.

EGGERS, J. & VILLERMAUX, E. 2008 Physics of liquid jets. *Rep. Prog. Phys.* **71**, 036601.

FARGIE, D. & MARTIN, B. W. 1971 Developing laminar flow in a pipe of circular cross-section. *Proc. R. Soc. Lond.* A **321**, 461–476.

FENN, R. W. & MIDDLEMAN, S. 1969 Newtonian jet stability: the role of air resistance. *AIChE J.* **12**, 379–383.

GAÑÁN-CALVO, A. M. 1998 Generation of steady liquid microthreds and micro-sized monodisperse sprays in a gas stream. *Phys. Rev. Lett.* **80**, 285–288.

GORDILLO, J. M. & GEKLE, S. 2010 Generation and breakup of Worthington jets after cavity collapse. Part 2. Tip breakup of stretched jets. *J. Fluid Mech.* **663**, 331–346.

GORDILLO, J. M. & PÉREZ-SABORID, M. 2005 Aerodynamic effects in the breakup of liquid jets: on the first wind-induced breakup regime. *J. Fluid Mech.* **541**, 1–20.

GOROKHOVSKI, M. & HERMMANN, M. 2008 Modeling primary atomization. *Annu. Rev. Fluid Mech.* **40**, 343–366.

GRANT, R. P. & MIDDLEMAN, S. 1966 Newtonian jet stability. *AIChE J.* **12**, 678–869.

GUILLOT, P., COLIN, A., UTADA, A. S. & ADJDARI, A. 2007 Stability of a jet in confined pressure-driven biphasic flows at low Reynolds number. *Phys. Rev. Lett.* **99**, 104502.

https://doi.org/10.1017/jfm.2014.329 Published online by Cambridge University Press

HIROYASU, H., ARAI, M. & SHIMIZU, M. 1991 Break-up length of a liquid jet and internal flow in a nozzle, *ICLASS-91, Gaithersburg, MD*, pp. 275–282.

HUERRE, P. & MONKEWITZ, P. A. 1990 Local and global instabilities in spatially developing flows. *Annu. Rev. Mech.* **22**, 473–537.

IBRAHIM, E. A. & MARSHAL, S. O. 2000 Istability of a liquid jet of parabolic velocity profile. *Chem. Engng J.* **76**, 17–21.

KARASAWA, T., TANAKA, M., ABE, K., SHIGA, S. & KURABAYASHI, T. 1992 Effect of nozzle configuration on the atomization of a steady spray. *Atomiz. Sprays* **2**, 411–426.

KELLER, J. B., UBINOW, S. L. & TU, Y. O. 1973 Spatial instability of a jet. *Phys. Fluids* **16**, 2052–2055.

LASHERAS, J. C. & HOPFINGER, E. J. 2000 Liquid jet instability and atomization in a coaxial gas stream. *Annu. Rev. Fluid Mech.* **32**, 275–308.

LE DIZES, S. 1997 Global modes in falling capillary jets. *Eur. J. Mech. (*B*/Fluids)* **16**, 166–182.

LEIB, S. J. & GOLDSTEIN, M. E. 1986 The generation of capillary instabilities on a liquid jet. *J. Fluid Mech.* **168**, 479–500.

LEROUX, S., DUMOUCHEL, C. & LEDOUX, M. 1997 The breakup length of laminar cylindrical jets: modification of Weber's theory. *Intl J. Fluid Mech. Res.* **24**, 428–438.

LIN, S. P. 2003 *Breakup of Liquid Sheets and Jets*. Cambridge University Press.

LIN, S. P. & LIAN, Z. W. 1989 Absolute instability of a liquid jet in a gas. *Phys. Fluids* A **1**, 490–493.

LIN, S. P. & REITZ, R. D. 1998 Drop and spray formation from a liquid jet. *Annu. Rev. Fluid Mech.* **30**, 85–105.

MARMOTTAN, P. & VILLERMAUX, E. 2004 On spray formation. *J. Fluid Mech.* **498**, 73–111.

MAYER, E. 1961 Theory of liquid atomization in high velocity gas stream. *Am. Rocket Soc. J.* **31**, 1783–1785.

MCCARTHY, M. J. & MOLLOY, N. A. 1974 Review of stability of liquid jets and influence of nozzle design. *Chem. Engng J.* **7**, 1–20.

MEISTER, B. J. & SCHEELE, G. F. 1967 General solution of the Tomotika stability analysis for a cylindrical jet. *AIChE J.* **13**, 682–688.

MONKEWITZ, P. A. 1990 The role of absolute and convective instability in predicting the behavior of fluid systems. *Eur. J. Mech. (*B*/Fluids)* **9**, 395–413.

MONKEWITZ, P. A., DAVIS, J., BOJORQUEZ, B. & YU, M. H. 1988 The breakup of a liquid jet at high Weber number. *Bull. Am. Phys. Soc.* **33**, 2273.

NELSON, P., POWER, T. & SEFFERT, U. 1995 Dynamic theory of pearling instability in cylindrical vesicles. *Phys. Rev. Lett.* **74**, 3384–3387.

O'DONNELL, B., CHEN, J. N. & LIN, S. P. 2001 Transition from convective to absolute instability in a liquid jet. *Phys. Fluids* **13**, 2732–2734.

PAN, Y. & SUGA, K. 2006 A numerical study on the breakup process of laminar liquid jets into a gas. *Phys. Fluids* **18**, 052101.

PHINNEY, R. E. & HUMPHRIES, W. 1973 Stability of a laminar jet of viscous liquid-influence of nozzle shape. *AIChE J.* **19**, 655–657.

PLATEAU, J. 1873 *Statique Experimentale et Theorique des Liquides Soumis aux Seules Forces Moleculaires*, vol. 2. Gauthier-Villars.

POWER, T. R. & GOLDSTEIN, R. E. 1997 Pearling and pinching: propagation of Rayleigh instabilities. *Phys. Rev. Lett.* **78**, 2555–2558.

RAYLEIGH, L. 1878 On the Instability of Jets. *Proc. Lond. Math. Soc.* **10**, 4–13.

REITZ, R. D. & BRACCO, F. V. 1986 Mechanisms of breakup of round liquid jets. In *The Encyclopedia of Fluid Mechanics* (ed. N. Cheremisnoff), vol. 3, pp. 233–249. Gulf.

RUBIO-RUBIO, M., SEVILLA, A. & GORDILLO, J. M. 2013 On the thinnest steady threds obtained by gravitational stretching of capillary jets. *J. Fluid Mech.* **729**, 471–483.

SCHULKES, R. M. S. M. 1996 The contraction of liquid filaments. *J. Fluid Mech.* **309**, 277–300.

SHINJO, J. & UMEMURA, A. 2010 Simulation of liquid jet primary breakup: dynamics of ligament and droplet formation. *Intl J. Multiphase Flow* **36**, 513–532.

https://doi.org/10.1017/jfm.2014.329 Published online by Cambridge University Press

SHINJO, J. & UMEMURA, A. 2011 Detailed simulation of primary atomization mechanism in diesel jet spray (isolated identification of liquid jet tip effects). *Proc. Combust. Inst.* **33**, 2089–2097.

SMITH, S. W. & MOSS, H. 1917 Experiments with mercury jets. *Proc. R. Soc. Lond.* A **43**, 373–393.

SPARROW, E. M., LIN, S. H. & LINDGREN, T. S. 1964 Flow development in the hydrodynamic entrance region of tubes and ducts. *Phys. Fluids* **7**, 338–347.

STERLING, A. M. & SLEICHER, C. A. 1975 The instability of capillary jets. *J. Fluid Mech.* **68**, 477–495.

STONE, H. A. & LEAL, L. G. 1989 Relaxation and breakup of an initially extended drop in an otherwise quiescent fluid. *J. Fluid Mech.* **198**, 399–427.

TAYLOR, G. I. 1959 The dynamics of thin sheets of fluid. III disintegration of fluid sheets. *Proc. R. Soc. Lond.* A **253**, 313–321.

TOMOTIKA, J. 1955 On the instability of a cylindrical thread of a viscous liquid surrounded by another viscous fluid. *Proc. R. Soc. Lond.* **150**, 322–337.

TYLER, E. & RICHARDSON, E. G. 1925 The characterisitic curves of liquid jets. *Proc. R. Soc. Lond.* A **37**, 297–311.

TYLER, E. & WATKIN, F. 1932 Experiments with capillary jets. *Phil. Mag.* **14**, 849–881.

UMEMURA, A. 2011 Self-destabilizing mechanism of a liquid jet issuing from a long nozzle. *Phys. Rev.* E **83**, 046307.

UMEMURA, A., KAWANABE, S., SUZUKI, S. & OSAKA, J. 2011 Two-valued breakup length of a water jet issuing from a finite-length nozzle under normal gravity. *Phys. Rev.* E **84**, 036309.

VIHINEN, I., HONOHAN, A. M. & LIN, S. P. 1997 Image of absolute instability in a liquid jet. *Phys. Fluids* **9**, 3117–3119.

WEBER, C. 1931 Zum Zerfall eines Flüssingkeitsstrahles. *Z. Angew. Math. Mech.* **11**, 136–145.

WU, P. K., MIRANDA, R. F. & FAETH, G. M. 1995 Effect of initial flow conditions on primary breakup of non-turbulent and turbulent round liquid jets. *Atomiz. Sprays* **5**, 175–196.

YECKO, P., ZALESKI, S. & FULLANA, J. M. 2002 Viscous modes in two-phase mixing layers. *Phys. Fluids* **14**, 4115–4122.

YECKO, P. & ZALESKI, S. 2005 Transient growth in two-phase mixing layers. *J. Fluid Mech.* **528**, 43–52.

https://doi.org/10.1017/jfm.2014.329 Published online by Cambridge University Press